The Mechanism Of Chlorine Incorporation In Silicon Dioxide During The Oxidation Of Silicon In Chlorine-containing Ambients.

Sheu, Yea-Dean

THE MECHANISM OF CHLORINE INCORPORATION IN SILICON DIOXIDE DURING THE OXIDATION OF SILICON IN CHLORINE-CONTAINING AMBIENTS

Lehigh University PH.D. 1985

PLEASE NOTE:

In all cases this material has been filmed in the best possible way from the available copy. Problems encountered with this document have been identified here with a check mark __✓__.

1. Glossy photographs or pages _____
2. Colored illustrations, paper or print _____
3. Photographs with dark background _____
4. Illustrations are poor copy _____
5. Pages with black marks, not original copy _____
6. Print shows through as there is text on both sides of page _____
7. Indistinct, broken or small print on several pages ✓
8. Print exceeds margin requirements _____
9. Tightly bound copy with print lost in spine _____
10. Computer printout pages with indistinct print _____
11. Page(s) _____ lacking when material received, and not available from school or author.
12. Page(s) _____ seem to be missing in numbering only as text follows.
13. Two pages numbered _____. Text follows.
14. Curling and wrinkled pages _____
15. Dissertation contains pages with print at a slant, filmed as received _____
16. Other _____

_____

_____

THE MECHANISM OF Cl INCORPORATION IN SiO_2 DURING THE OXIDATION OF Si IN Cl-CONTAINING AMBIENTS

Yea-Dean Sheu

A Dissertation
Presented to the Graduate Committee
of Lehigh University
in Candidacy for the Degree of
Doctor of Philosophy
in
Metallurgy and Materials Engineering

Lehigh University
1985

Approved and recommended for acceptance as a dissertation in partial fulfillment of the requirements for the degree of Doctor of Philosophy.

August 27, 1985
Date

Sidney R Butler
Professor in Charge

Accepted 8/27/85
(Date)

Special committee directing the work of Yeadean Sheu

Sidney R Butler
Chairman

Ralph J Jansen

Dru Smith

ACKNOWLEDGEMENT

I would like to express my sincere gratitude to Professor S. R. Butler, my advisor, for his continuous assistance, guidance, and patience. I would also like to thank Professors F. J. Feigl, D. M. Smyth, and R. J. Jaccodine for serving as members of my dissertation committee. The assistance of and discussions with Professor Feigl were particularly valuable.

I also wish to thank Dr. C. W. Magee of RCA Laboratories and Dr. R. O. Gale of Central Research Laboratory, Texas Instruments, for the SIMS measurement. Thanks are also expressed to Drs. Taeho Kook, Hongzong Chew, and Ajeet Rohatgi of for their assistance at various stages of this dissertation. Support from the Physics Department of Lehigh University, National Science Foundation, and Sherman Fairchild Foundation are gratefully acknowledged.

Finally, I wish to express my eternal gratitude to my mother for her moral support and my wife Ching-Yee for her sacrifice and understanding which made it all possible.

Table of Contents

List of Figures

List of Tables

ABSTRACT

Cl was introduced into SiO_2 films by either thermally oxidizing the Si in HCl/O_2 or Cl_2/O_2 ambients at 1100°C or implanting ^{35}Cl. Cl concentration vs. depth profiles were determined by secondary ion mass spectrometry (SIMS). Analysis of the SIMS profiles shows the Cl incorporation in HCl oxides is due to both HCl and Cl_2. H_2O interferes with these incorporation processes. Replacement of the bonded Cl in HCl oxides is quantitatively modeled by the kinetics of the chemical reaction by which OH replaces Cl. The replacement reaction is shown to have faster kinetics when H_2O is present than when only oxygen is present by comparing the Cl profile in HCl and Cl_2 oxides. The redistribution of the bonded Cl (i.e. the implanted Cl in SiO_2 or the Cl incorporated by thermally oxidizing the Si in Cl-containing ambients) during subsequent heat treatment was shown to be consistent with these reaction models. These observations indicate that the Cl concentration vs. depth profiles are determined by chemical reactions involving Cl, H_2O, and O_2.

Chapter 1

Introduction

Oxidation of Si in chlorine-containing ambients is a widely used process in preparing the gate oxides for Si devices (1). This process can passivate Na ions in the oxide (2), suppress the growth of the oxidation-induced stacking faults (3), produce better reproducibility in breakdown voltages (4), and enhance the oxidation kinetics (5). In this process Cl is incorporated into the SiO_2, and is found to be primarily segregated near the Si/SiO_2 interface (6-8). Recent Cl concentration versus depth profiles determined by secondary ion mass spectrometry (SIMS) show a significant amount of Cl distributed in the oxide with increasing concentration toward the Si/SiO_2 interface (9-13). One interpretation of these profiles was that the measured Cl was the mobile, diffusing Cl species (11). The authors suggested that the Cl transport was by a "field-aided" diffusion process, against the concentration gradient. However, the origin of such a field was not established. In contrast, we suggested this profile was determined by a reaction-controlled process (13,14). This difference has not been resolved. In addition, both HCl and Cl_2 should be present in the oxidation ambients of HCl/O_2 mixtures due to

the gas-phase reaction of the HCl and O_2 (15). Therefore a question remains concerning the active species driving the Cl incorporation in this type of oxidation.

A Cl-rich phase has been observed to form at the Si/SiO_2 interface in highly chlorinated oxides, and it was suggestsed that the chlorine incorporation is primarily the result of this Cl-rich phase formation (16). A model based on the thermodynamic stability of this phase, as determined by the activities of competing oxidants was suggested to account for the Cl-rich phase development (17). However, detailed studies with the analytical electron microscope found Cl incorporation in the matrix without Cl-rich phase formation (13). The Cl-rich phase was found to form only when the Cl areal density was above $2x10^{15}cm^{-2}$. To avoid the complexity of the Cl-rich phase development, the majority of the present study was limited to Cl concentration below this value.

Overview of Experimental Program and Results

The Cl was introduced into the SiO_2 either by ion implantation or by thermally oxidizing the Si in Cl-containing ambients. The oxides were then heat-treated in various ambients to study the effect of the ambients on the redistribution of the bonded Cl. The Cl concentration as measured by secondary ion mass spectrometry

(SIMS), shows the Cl is strongly segregated to the Si/SiO_2 interface during the oxidation. These results also show that the redistribution of the Cl is a reaction-controlled process, not a diffusion-controlled process.

Exchange of the oxidants with the SiO_2 network during the thermal oxidation in H_2O or H_2O containing ambients is well established (18,19). O_2 exchange with the SiO_2 network was observed recently (20). Similarly, H_2O and O_2 are also known to replace the Cl in the network (21,22). In order to see how these replacement reactions can affect the Cl during the oxidation, samples are prepared by a sequence of oxidations for different times at fixed temperature and HCl/O_2 mixing ratio. The measured Cl profiles of these samples show that at a position fixed with respect to the outer oxide surface, the Cl concentration decreases as oxidation proceeds due to the above-mentioned replacement reactions.

In order to determine the active species responsible for Cl incorporation in HCl oxidations, oxides were prepared in several different ambients such that the roles of HCl, Cl_2, and H_2O are evident. To clarify the effect of H_2O in HCl oxidation, oxides were prepared in Cl_2/O_2 ambients with the same Cl_2 partial pressure as that in the above-mentioned oxidations in $HCl-O_2$ ambients.

As the above results show, Cl is incorporated into

the SiO_2 primarily at the Si/SiO_2 interface, and, as an approximation, the interfacial Cl concentration can be assumed constant. The incorporated Cl is replaced by OH via the reaction with H_2O as the interface moves away during the subsequent oxidation process. The concentration profile for the O_2, H_2O and HCl during oxidation can be determined with the steady state approximation (5,23).

A simple kinetic model based on the replacement reaction

$$-\overset{|}{\underset{|}{Si}}-Cl + H_2O \rightleftharpoons -\overset{|}{\underset{|}{Si}}-OH + HCl$$

and the concentration profile of the diffusants in the oxide will be introduced to explain these Cl profiles. The reaction rate constant can be obtained by fitting the Cl concentration profiles to this model.

These results will be discussed with the objective of understanding the several processes that determine the chlorine incorporation.

Chapter 2

Experimental and Results

2.1 Sample Preparation and Results

2.1.1 Oxidation in Cl-containing Ambients

Oxides were prepared by oxidizing high resistivity (100) Si in Cl-containing ambients at 1100°C for 20, 40, and 160 minutes.

As shown in Figure 2-1, the Cl addition to the oxidation ambient was carried out by flowing a controlled amount of O_2 through a bubbler at room temperature containing either liquid TCA [$C_2H_3Cl_3$] for HCl type oxidations or CCl_4 for Cl_2 type oxidations. In this study the samples prepared by these two processes will be referred to as HCl type oxides and Cl_2 type oxides, respectively. In order to confirm that the carrier gas was saturated with the vapor to be added, the effluent from the bubbler was passed through a desiccant ($CaSO_4$) trap for one hour and the weight increase was determined. The measured value is 97% of that calculated for saturation. Assuming $C_2H_3Cl_3$ decomposes completely to HCl and CO_2 at elevated temperature (24) as does CCl_4 to Cl_2 and CO_2 (25), the flow rate of the carrier gas can be determined by

$$\frac{1/3 \times (760 - P_{TCA})}{P_{TCA}}$$

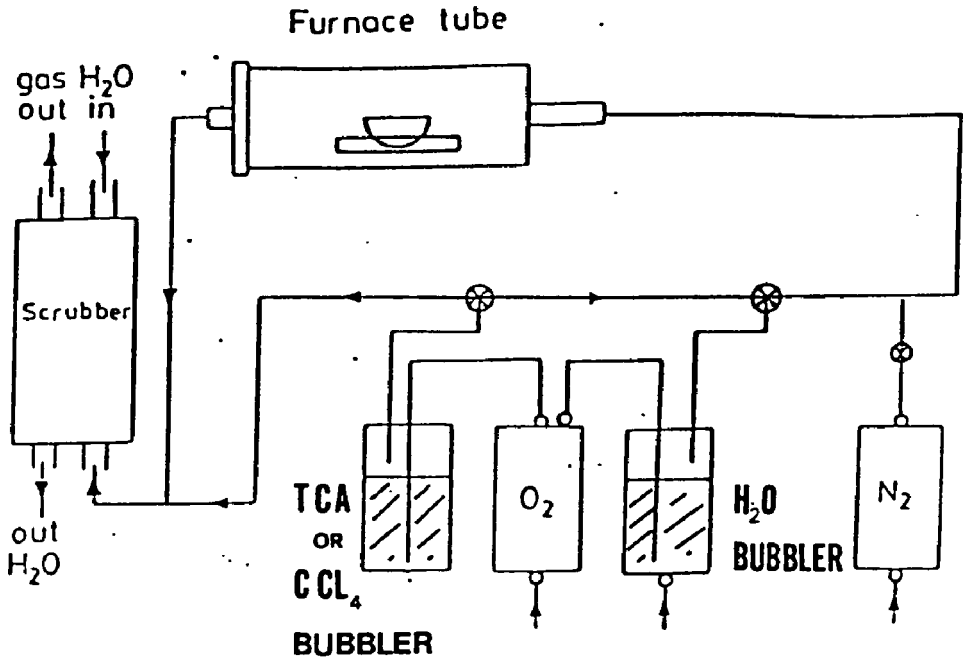

Fig. 2-1 Schematic diagram of TCA or CCl_4 oxidation apparatus.

for HCl oxides, and

$$\frac{1/2 \times (760 - P_{CCl_4})}{P_{CCl_4}}$$

for Cl_2 oxides. Where X is the desired composition, P_{TCA} and P_{CCl_4} are the vapor pressure of liquid $C_2H_3Cl_3$ and CCl_4 at room temperature, respectively. The addition of H_2O to the oxidation ambient was carried out in similar manner, and saturation checked in a similar way.

For HCl oxides, two sets of oxidation ambients were prepared on the basis of thermodynamic calculations (26) such that the HCl partial pressure was held constant while the Cl_2 partial pressure varied by a factor of about 4, or the inverse; i.e., the Cl_2 partial pressure was constant and the HCl varied. Table 2-1 lists the initial mixture compositions and high temperature gas-phase partial pressures in these two sets of ambients. Note that the H_2O partial pressure must be varied in order to keep HCl or Cl_2 partial pressure constant.

The Cl_2 oxides were prepared in O_2 plus 0.15% and 0.30% Cl_2. As Table 2-1 shows, 0.15% and 0.30% Cl_2 are the equilibrium Cl_2 concentration for the initial mixture of O_2 plus 1% HCl and 2% HCl at 1100°C, respectively. Effluent from the oxidation chamber was passed through a P_2O_5 electrolytic surface conductivity cell made by

Table 2-1

Equilibrium Partial Pressure and Total Cl for

$O_2/TCA/H_2O$ and O_2/CCl_4 Mixture at 1100°C

Identifying Letter	Initial Mixture (%)*		Equilibrium Partial** Pressure (10^{-3} atm)			Total Cl ($10^{14}/cm^2$) Oxidation Time (minutes)		
	H_2O	$C_2H_3Cl_3$	P_{HCl}†	P_{Cl_2}	P_{H_2O}	20	40	160
A	0	0.67	14.0	3.0	3.0	11.0	18.9	33.2
B	0.25	0.60	14.0	2.0	4.5	5.7	10.2	16.3
C	1.0	0.53	14.0	0.87	10.0	2.4	4.0	5.8
D	0	0.33	7.0	1.5	1.5	6.1	10.2	22.4
E	0.7	0.67	17.0	1.6	8.6	4.2	4.5	13.6
F	2.0	1.0	27.0	1.6	22.0	2.4	3.8	8.1

(Continued)

Table 2-1 (Continued)

	CCl_4	P_{Cl_2}	20	40	160
G	1.5	3.0	16.0	24.1	42.7
H	0.75	1.5	7.1	13.4	22.4

*Total pressure = 1.0 atm; remainder is O_2.

†We assume $C_2H_3Cl_3$ decomposes completely to HCl and CO_2; i.e., 0.67% $C_2H_3Cl_3$ corresponds to 2% HCl (15). A similar assumption is made concerning the decomposition of CCl_4 to CO_2 and Cl_2 (16).

**The chemical reaction considered for this equilibrium calculation is:

$$4HCl + O_2 \rightleftarrows 2H_2O + 2Cl_2$$

Manufacturers Engineering & Equipment Corporation of Warrington, PA. This instrument measures moisture content to levels below 1 ppm. The measured moisture content was approximately 3 ppm after flowing the oxygen through the 1100°C furnace at 1 liter/min for one hour. The value dropped to approximately 0.5 ppm when the Cl was introduced into the oxidation furnace presumably due to the reaction between Cl and H_2O to form HCl.

The Si wafers to be oxidized were cleaned by boiling in trichloroethylene, methanol and acetone sequentially. Immediately before the oxidation the wafers were lightly etched in 10:1 dilute HF to remove any traces of native oxide, rinsed in DI water, and blown dry in nitrogen. These cleaned Si wafers were pushed rapidly into a silica tube in a resistance heated furnace and allowed to stand for 5 minutes in flowing nitrogen for thermal equilibration. The temperature of the furnace had been profiled such that it was within 0.5°C of the desired temperature over the central zone of the furnace. Oxidation was started by shutting off the inert gas and turning on the mixture of HCl and O_2 with a preestablished volume mixing ratio with the method as described above. The flow rate of the gases were monitored by flow meters and the total flow rate was kept at 1 liter/min. At the end of oxidation, the O_2/HCl or Cl_2 flow was stopped, the furnace was purged with

nitrogen at 2 liters/min for 10 minutes, and then the wafers were pulled out of the furnace rapidly. The oxide thickness of all samples was determined by ellipsometry (36). A Rudolph Auto EL-II ellipsometer was used for these measurements. Secondary Ion Mass Spectrometry (SIMS), as described later, was used for chemical analysis in this study.

The oxide thickness of the HCl and Cl_2 oxides are shown in Table 2-2. Figure 2-2 shows the Cl concentration versus depth profiles in the oxides grown in 2% HCl and in 0.30% Cl_2 for several oxidation times. The uniform oxygen signal indicates the constant sensitivity throughout the sputtering process. The overall depth resolution is estimated to be about 5 nm. This value is determined from the drop in the oxygen signal at the Si/SiO_2 interface (37). The Cl concentration versus depth profile of the other HCl and Cl_2 oxides is shown in Appendix I. The areal density of Cl (i.e. the area under the Cl concentation vs. depth curve) for the HCl and Cl_2 oxides is tabulated in Table 2-1 and summarized in Figure 2-3.

As Fig. 2-2(d) shows, for a typical case, the measured hydrogen concentration in the 1 and 2% HCl oxides was always found to be in the range from 10^{20} to 10^{21} cm^{-3}. The profiles were nearly flat in the bulk

Table 2-2

Equilibrium Partial Pressure and Oxide Thickness for Oxidation in $O_2/TCA/H_2O$ and O_2/CCl_4 Mixture at 1100°C

Initial Mixture (%)		Equilibrium Partial Pressure (10^{-3} atm)			Oxide Thickness (Å)		
H_2O	$C_2H_3Cl_3$	P_{HCl}	P_{Cl_2}	P_{H_2O}	20* (min)	40 (min)	160 (min)
0	0.67	14.0	3.0	3.0	833	1239	2640
0.25	0.60	14.0	2.0	4.5	807	1213	2590
1.0	0.53	14.0	0.87	10.0	837	1237	2630
0	0.33	7.0	1.5	1.5	748	1193	2518
0.7	0.67	17.0	1.6	8.6	821	1252	2635
2.0	1.0	27.0	1.6	22.0	897	1339	2848

	CCl_4	P_{Cl_2}	20	40	160
	1.5	3.0	870	1285	2787
	0.75	1.5	792	1170	2650

* Oxidation time.

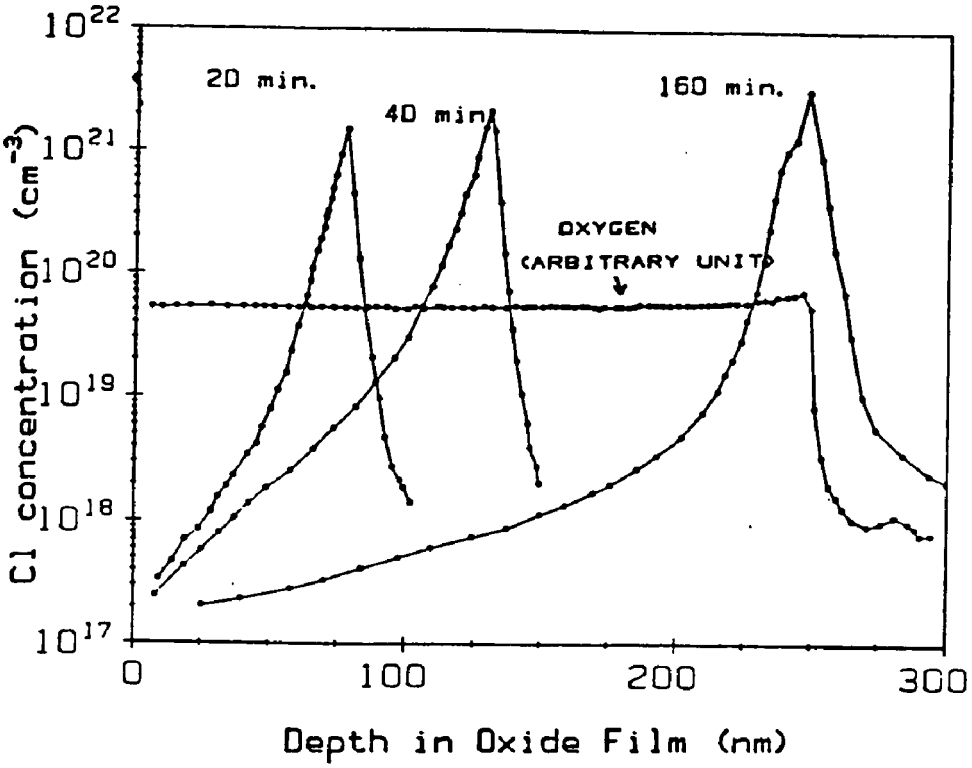

Fig. 2-2(a) Chlorine profiles for samples prepared by oxidation at 1100°C in 2% HCl ambients.

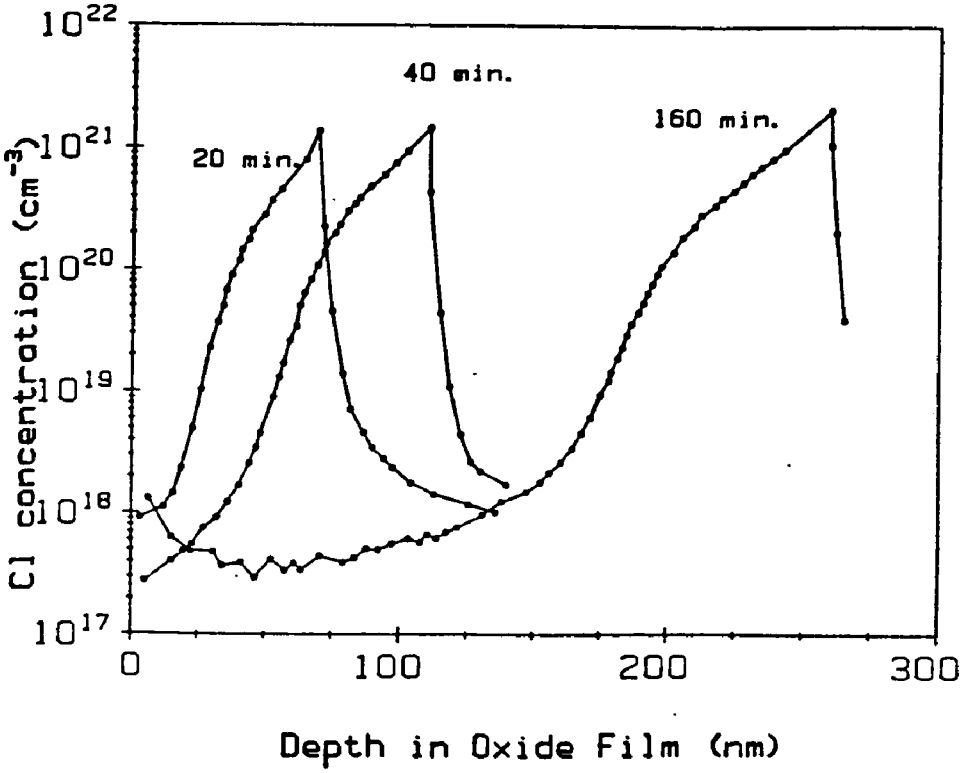

Fig. 2-2(b) Chlorine profiles for samples prepared by oxidation at 1100°C in 0.30% Cl_2 ambients.

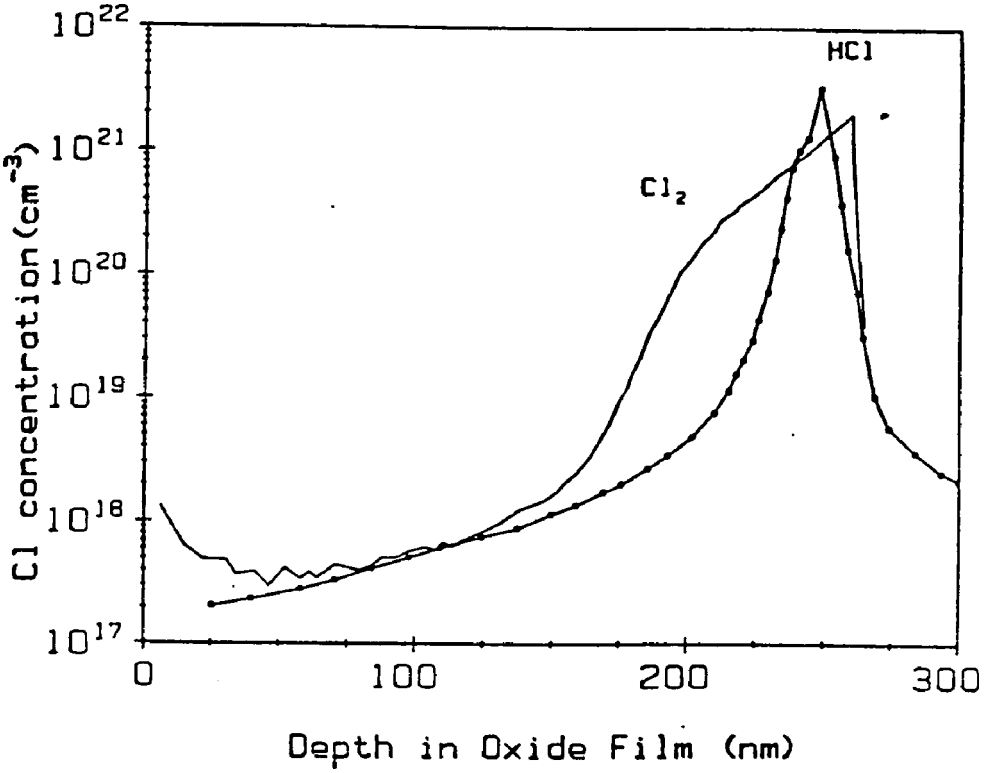

Fig. 2-2(c) A comparison of the two types of oxides for 160 minute oxidations.

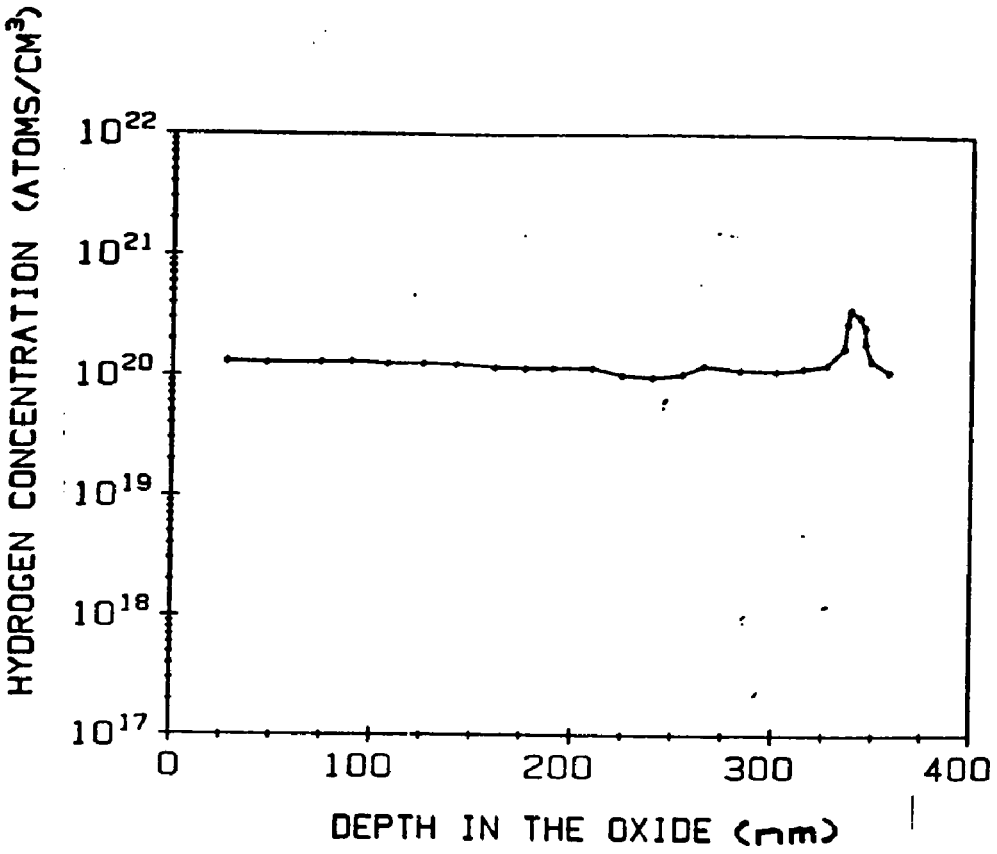

Fig. 2-2(d): Hydrogen concentration vs. depth profile for sample prepared by oxidation at 1100°C in 2% HCl ambients.

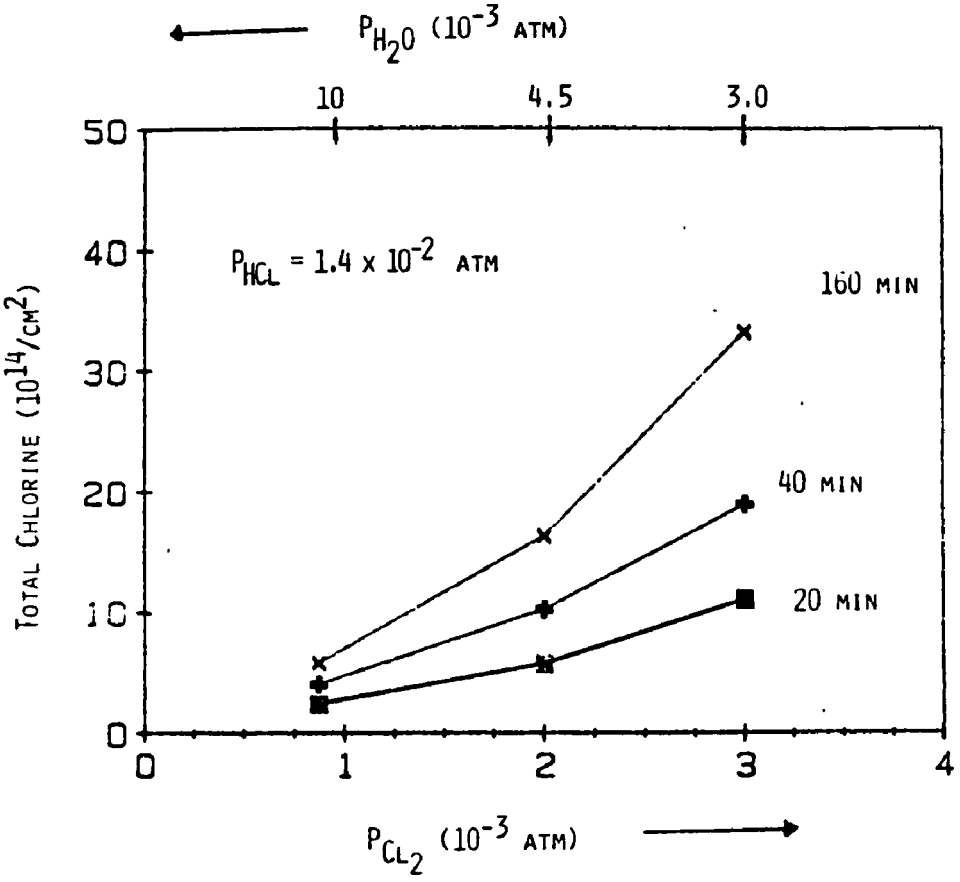

a

Fig. 2-3 Total chlorine content of samples prepared at 1100°C in $C_2H_3Cl_3$-H_2O-O_2 mixtures. The mixtures are adjusted to keep the HCl pressure constant while the Cl_2 pressure increases, a, or the reverse in b. Calculated H_2O partial pressures are given for the specific condition used.

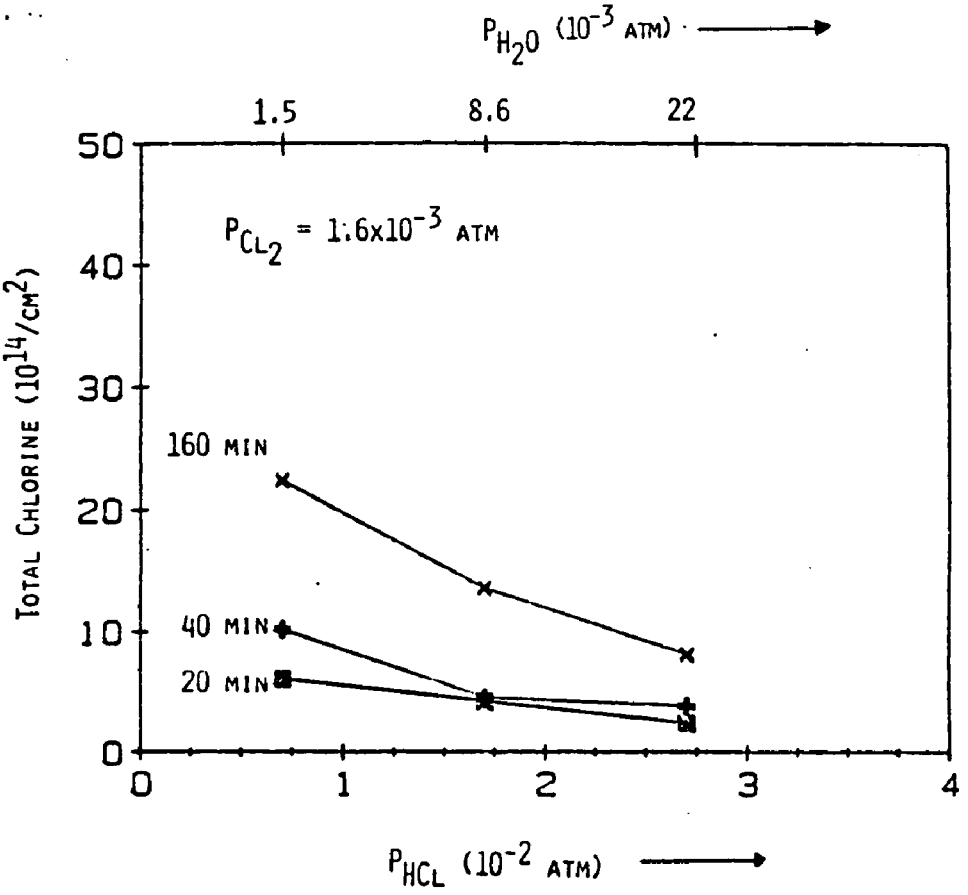
P_{H_2O} (10^{-3} ATM)
1.5
8.6
22
50
40
30
20
10
0
P_{CL_2} = 1.6x10^{-3} ATM
160 MIN
40 MIN
20 MIN
TOTAL CHLORINE (10^{14}/CM^2)
0
1
2
3
4
P_{HCL} (10^{-2} ATM)

b

oxide with a small peak at the Si/SiO_2 interface. This is very similar to the results previously reported in (12).

2.1.2 Annealing of the Bonded Cl in SiO_2

Cl-implanted oxides were provided by Dr. A. Rohatgi of Westinghouse Research Laboratory.

The Cl was implanted into SiO_2 films of thickness 260 nm by implanting ^{35}Cl at 115 keV to a dose of $5x10^{13}$ cm^{-2}. The implanted energy and dose were selected such that most of the Cl was in the central portion of the oxide and the Cl concentration did not exceed its estimated solubility limit in the oxide. After implantation, the samples were annealed in nitrogen at 600°C for 30 minutes to remove the radiation damage (27,28). The samples were then given an additional oxidation separately for 20, 40, and 60 minutes at 900°C in either dry oxygen [H_2O = 2 ppm], O_2 with 2% H_2O, or wet O_2 [i.e. O_2 bubbled through water at 95°C].

Figure 2-4(a) shows the initial Cl profile (i.e. as-implanted and annealed at 600°) and the profiles after annealing 20 minutes in the ambients as described above. The raw data for annealing in wet O_2 is shown in Fig. 2-4(b). In this case, no Cl was detected with concentration higher than the background level. The resultant profiles for 40 and 60 minutes annealing are shown in Appendix II.

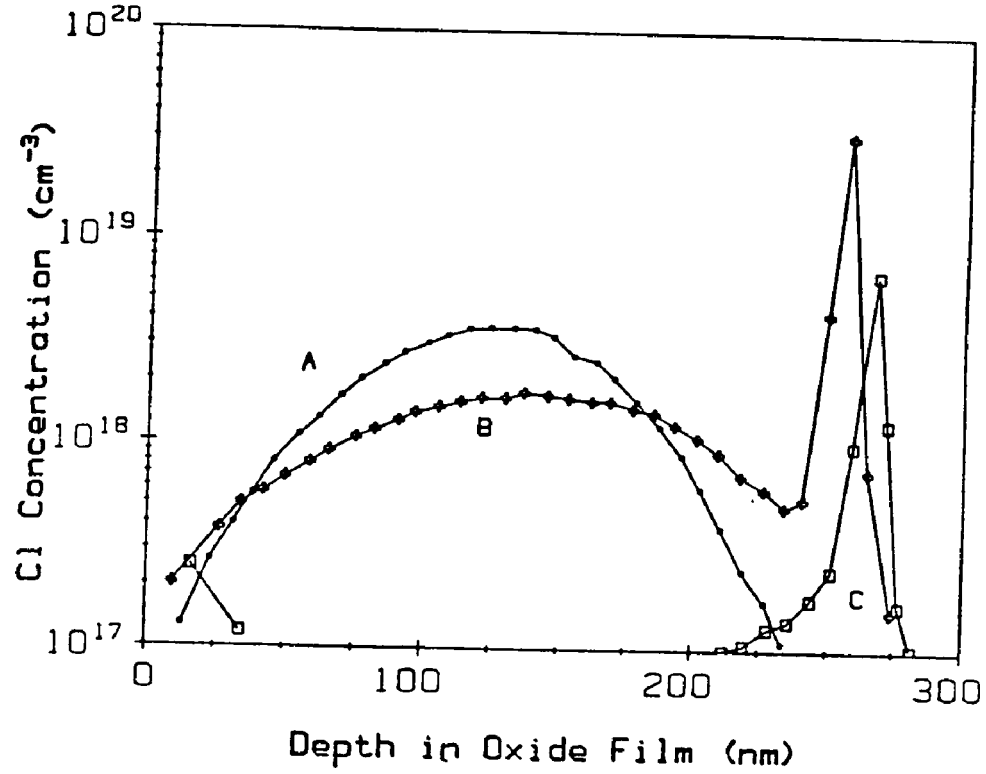

Fig. 2-4(a) Chlorine concentration vs. depth profiles for CL implanted oxides. Dose = $5x10^{13}$ atoms/cm^2. All samples annealed at 600°C for 30 minutes in N_2. Subsequent oxidations: A, none (x_o = 264 nm); B, 900°C for 20 minutes in dry O_2 (x_o=266 nm); C, 900°C for 20 minutes in O_2 + 2% H_2O (x_o=268 nm).

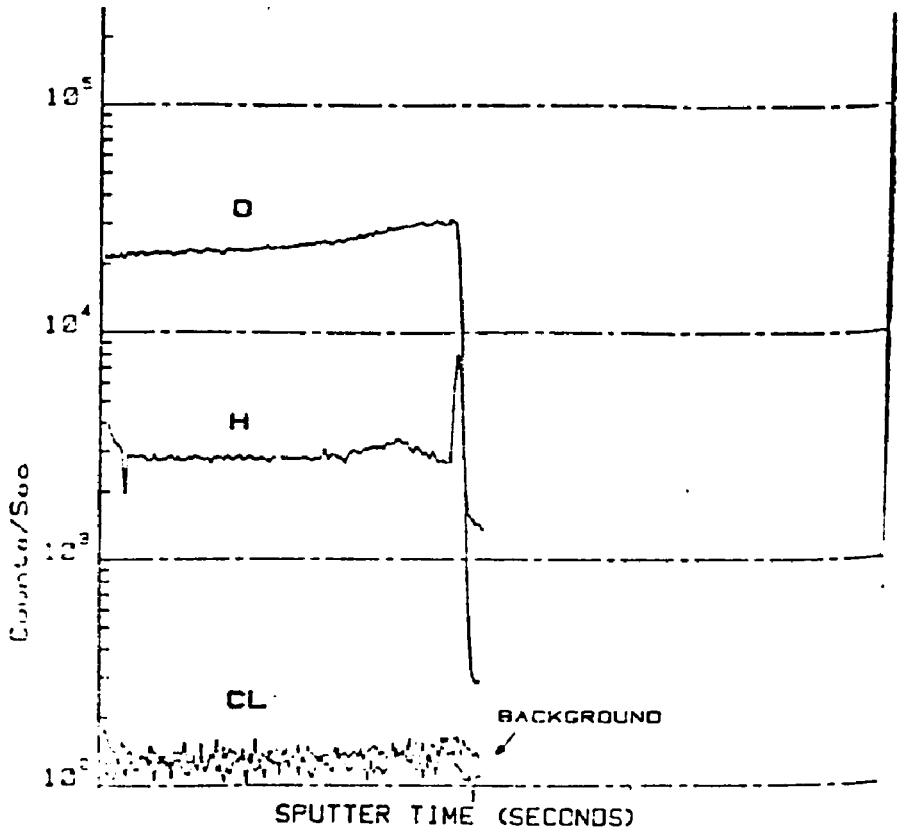

Fig. 2-4(b) Chlorine concentration vs. depth profiles for Cl implanted oxides. Dose = 5×10^{13} atoms/cm^2. All samples annealed at 600°C for 30 minutes in N_2. Subsequent oxidation in wet O_2 for 20 minutes.

Following growth in HCl/O_2 ambients, some oxides had Cl implanted in them. A typical Cl concentration vs. depth profile for those oxides is shown in Fig. 2-5(a). For the purpose for which this data set will be used, the implanted Cl will be ignored. These oxides were then heat-treated in O_2 with 2% H_2O, and wet O_2. The initial and resultant profiles after these heat-treatments for 20 min. were shown in Figure 2-5(b). Appendix V shows the resultant profiles for 40 and 60 min. annealings. The raw data for heat-treatment in wet O_2 is shown in Fig. 2-5(c).

2.2 Chlorine Concentration Measurements

The chemical analysis in this study was performed by Dr. C. W. Magee of RCA Laboratories using Secondary Ion Mass Spectrometry (SIMS). The overall view of the RCA SIMS instrument is shown in Figure 2-6. The construction and performance of the instrument have been described in detail in (29) and summarized in (30). The following description of the SIMS technique draws heavily on these two references.

2.2.1 Brief Outline of SIMS Technique

Primary Ion Beam: Positive ions are created in the ion gun by an arc discharge in an inert gas ambient (^{40}Ar). Some of the ions formed are extracted from the source region, accelerated to 5 KeV, then focused by the first einzel lens. The first set of deflection plates

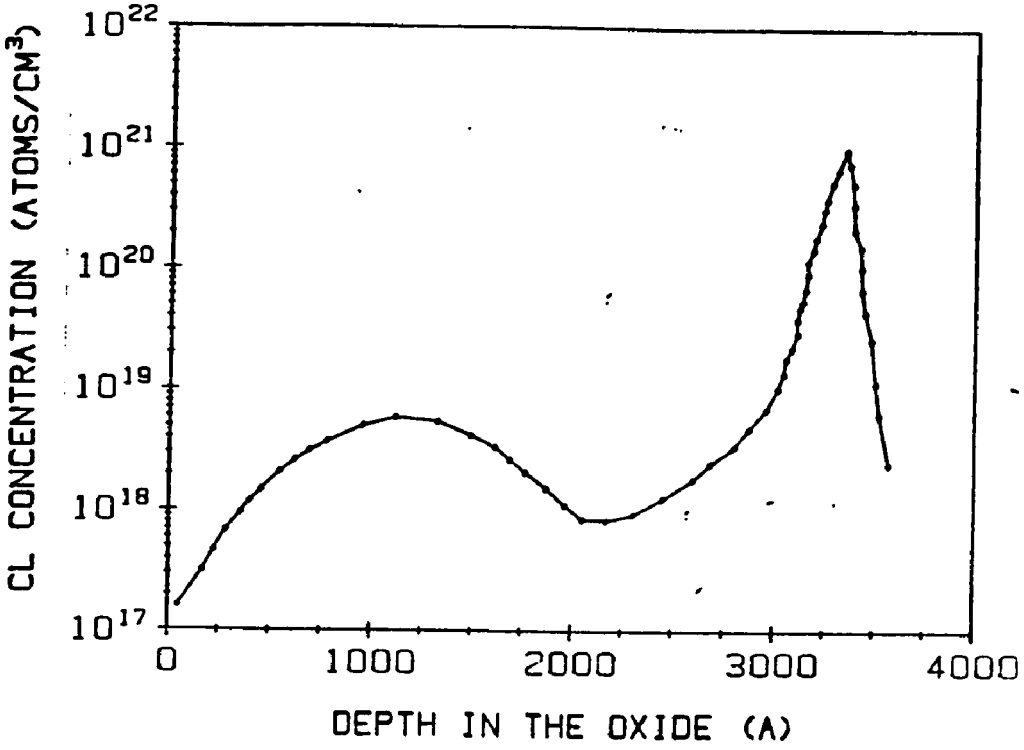

Fig. 2.5(a) Initial profile. See text on page 23 .

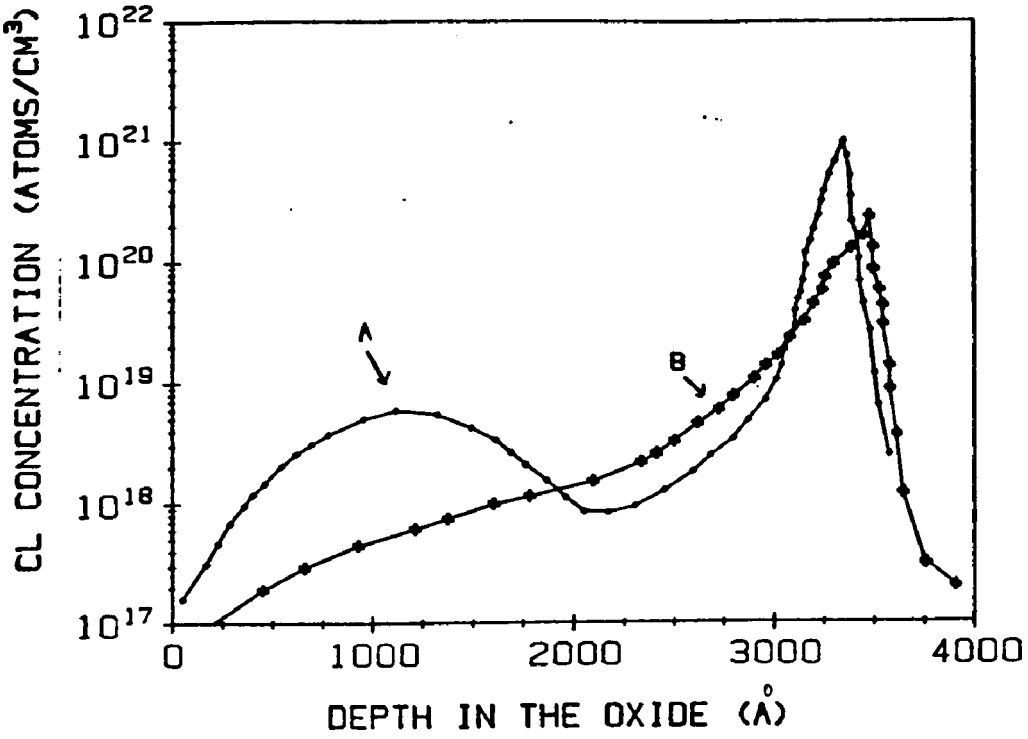

Fig. 2.5(b) A: Initial profile
B: Annealing in O_2 + 2% H_2O for 20 min. at 900°C.
See text on page 23 .

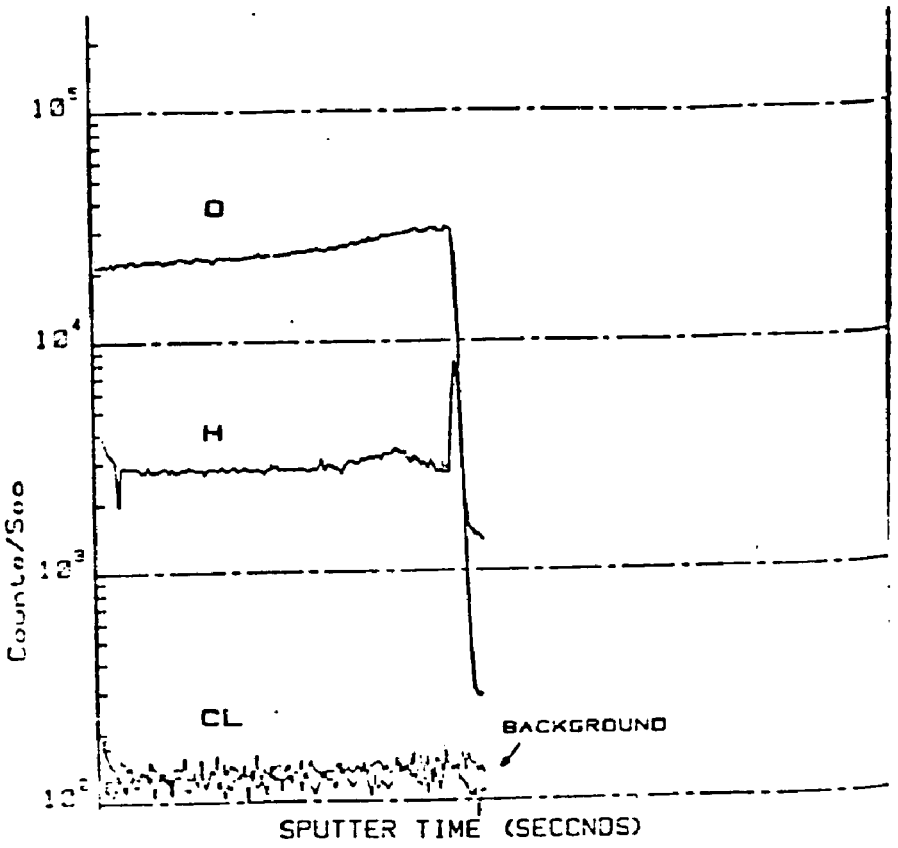

Fig. 2.5(c) Annealing in wet O_2 for 20 min at 900°C.

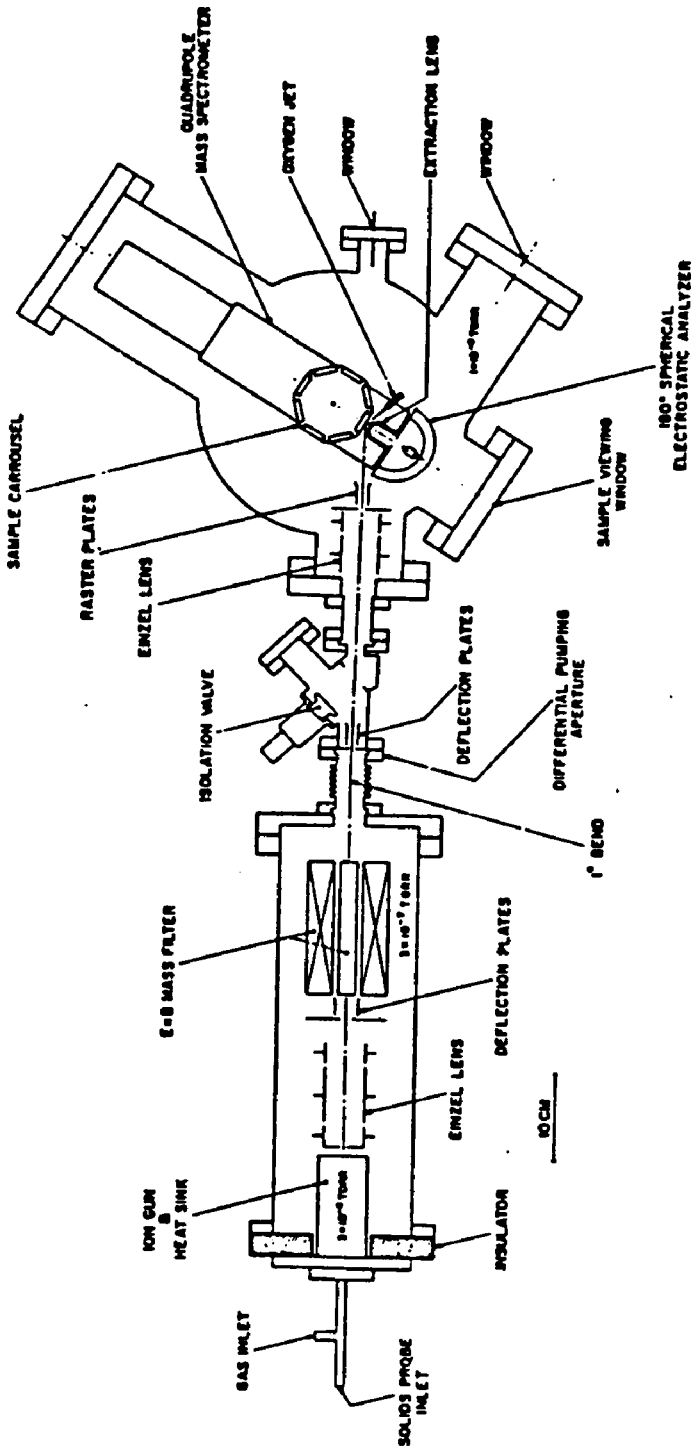

Fig. 2-6 Plan view of SIMS instrument used for chemical analysis in SiO_2. Reproduced from Magee, et al. (31).

guides the beam into the Wien (ExB) filter which passes undeflected ions of a particular mass to charge ratio. A second set of deflection plates in conjunction with a 1^{o} bend in the beam line separates neutrals from the beam. The second einzel lens focuses the beam on the sample surface with an angle of incidence of 60^{o} from the surface normal. Typical primary beam is operated at 400 to 700 na with a beam size of 50μm.

The primary beam erodes the sample surface by momentum transfer in the outermost atom layers of the sample. The penetration depth of the primary beam and the sputtering rate depend strongly on the primary species and the sample composition, as well as the primary energy and current density. A small fraction of the sample atoms sputtered away by the primary beam are ionized, either positively or negatively. This fraction depends on the primary species, the secondary species, the surrounding sample matrix, and the surface chemistry of the sample.

In order to accurately measure concentration profiles by SIMS, the information acquired must come from a well-defined narrow sample depth. This instrument uses the primary ion beam rastering to produce a flat crater bottom parallel to the original sample surface. To further improve the depth

resolution, simultaneous signal-gating is used. This gating activates the secondary ion detection electronics only when the rastering primary beam strikes the sample in the central flat bottom region of the crater. Since the matrix is insulating SiO_2, the charge build up during the sputtering process must be minimized by a neutralization electron beam (31).

Secondary Ion Optics: Figure 2-7 shows a detail of the secondary ion collection and analysis apparatus. The secondary ion optical axis is normal to the sample surface. The extraction lens focuses only ions originating in the central region of the sputtered crater on the entrance aperture of the energy analyzer. The hemispherical energy analyzer produces the narrow energy distribution (1-2 ev) necessary for good mass separation in quadrupole mass analyzers, and compensates for the chromatic aberration of the extraction lens. Secondary ions of the selected mass to charge ratio are transmitted by the quadrupole mass analyzer to a sixteen stage electron multiplier. Pulse output is routed to a high speed electronic counter. In addition, the unique design of the secondary ion optics in this instrument allows negative as well as positive ions to be detected (12). Since Cl atom is much more likely to be sputtered as Cl^- than Cl^+, higher sensitivity should be achievable if Cl^- is monitored. The intensity of selected ions

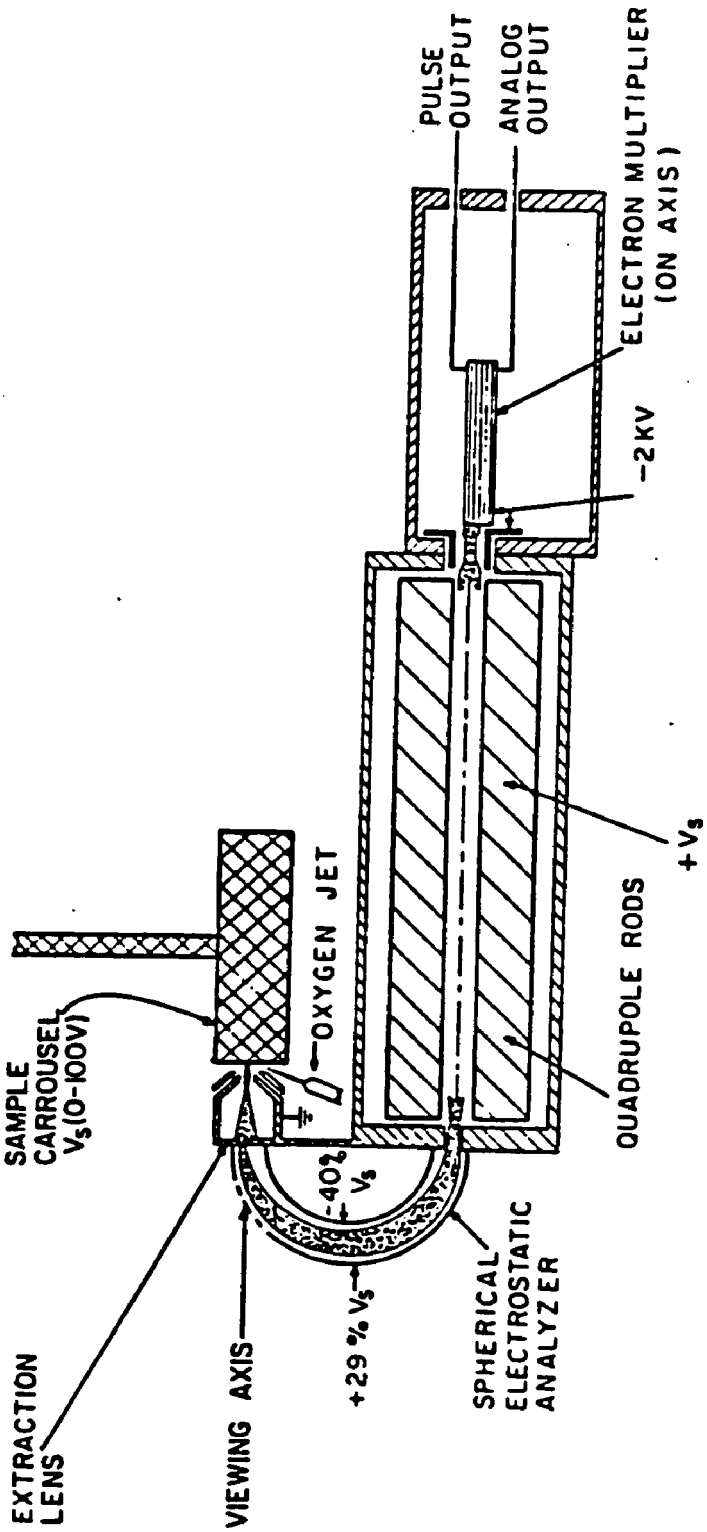

Fig. 2-7 Details of secondary ion extraction optics in RCA SIMS Instrument (after Magee, ref. 31).

may be monitored as the sample is sputtered at constant rate to yield a concentration profile of the selected ions as a function of time after calibrating by the procedures to be described later.

Summary: The oxides were analyzed by SIMS using a rastered 400 to 700 nA, 5 keV $^{40}Ar^{+}$ sputtering beam. The negative secondary ions were monitored. Electron-beam charge neutralization was used.

2.2.2 Calibration of SIMS Analysis

A typical set of raw data from a SIMS analysis is shown in Figure 2-8. In this figure count rate is plotted as a function of sputtering time. Calibration is required to convert time scale into depth scale and count rate into volume concentration by the following procedures.

Depth Calibration: The Si/SiO_2 interface is located where the oxygen signal drops abruptly. Thus the sputtering rate can be determined from the oxide thickness measured by ellipsometry and the sputtering time up to the Si/SiO_2 interface. In this way the time scale can be converted into depth scale provided the sputtering rate is constant.

Concentration Calibration: Quantification in SIMS analysis involves the use of ion-implanted standards to establish the absolute sensitivity of the instrument for

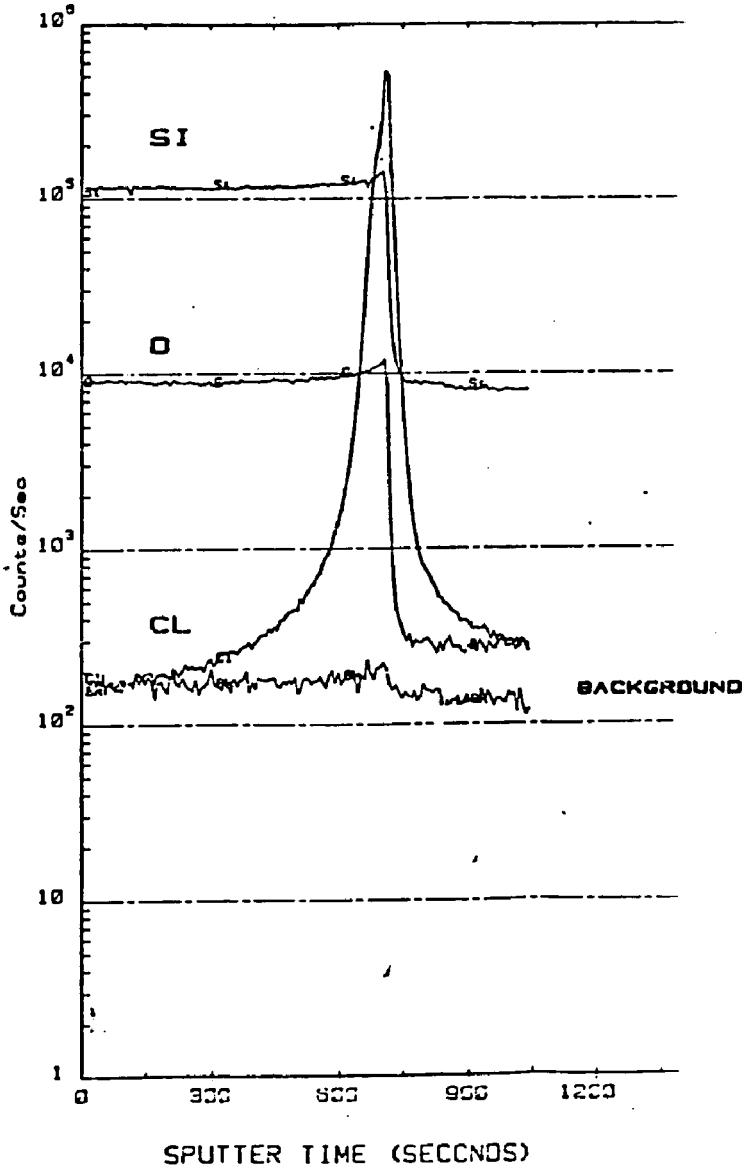

Fig. 2-8 Raw data for the oxides grown in 2% HCl at 1100°C for 160 min.

the ion of interest (33). The standard used in this work was 180 KeV $^{35}Cl^{+}$ implanted into SiO_2 of approximately 1μm thickness (SIMS profile shown in Figure 2-9).

After background correction, the Cl ion count rate vs. sputtering time data for the standard were integrated numerically to obtain the total number of Cl ions detected. The number of Cl atoms sputtered from the analyzed volume was calculated as the product of the gated area (the area from which Cl ion signals were accepted) and the implant dose. The ratio (atoms sputtered)/(ion detected) is of the order of 10^6. Volume concentration can be calculated by dividing atoms/sec by analyzed volume removed per second. The analyzed volume removal rate was calculated as the product of linear sputtering rate and the gated area.

The calibration of RCA SIMS has been done using Cl implants with doses of $1x10^{14}$, $3x10^{14}$, and $1x10^{15}$ cm^{-2}. The calibrations agree so well that only one dose is required (9). To demonstrate the reproducibility of this instrument, a sample was reanalyzed after one month. The Cl profiles of these two samples are shown in Figure 2-10.

In this study, a standard provided from a second source (A. Rohatgi of Westinghouse Research

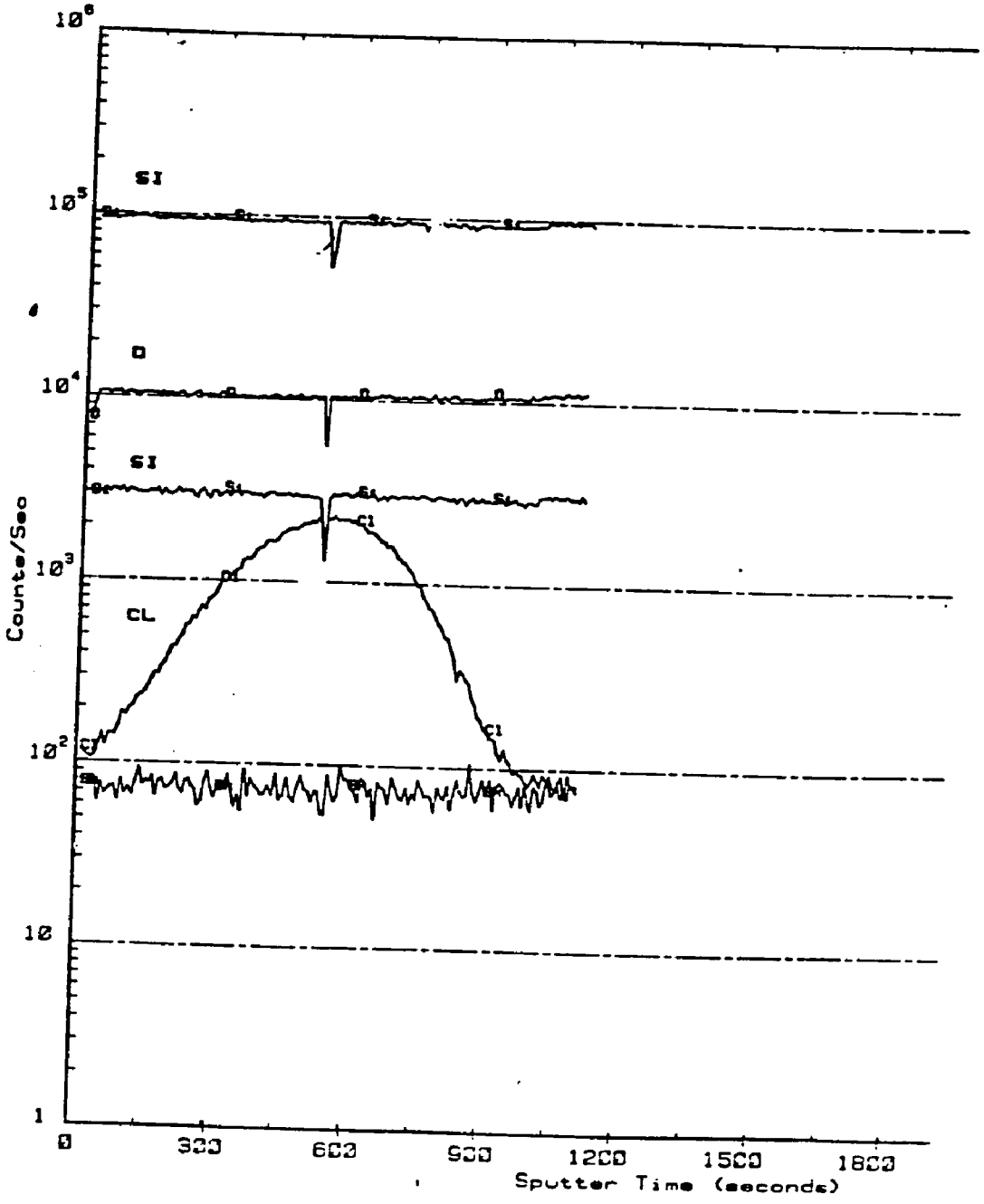

Fig. 2-9 Raw data for the standard for the calibration.

Laboratories) has been used to check the calibration constant. The difference in the calibration of these two standards is approximately 20%. This value agrees with the estimation of the accuracy for the concentration obtained in SIMS analysis (7). It is attributed to the uncertainty in the exact dose and lateral nonuniformity of the ion-implanted standard.

Small changes in the ion optical axis geometry can affect sensitivity. Matrix signals are used to compensate for these effects. A matrix signal is the ion count rate from one of the major constituents of the sample. Since the matrix element concentration is constant in samples of the same material, the observed count rate should be the same. The normalization factor required to make the matrix signal the same in two different samples is applied to the signal of interest (chlorine). In this study, oxygen is used as a matrix signal for the normalization.

Appendix III shows the full calculations required to convert the raw data shown in Figure 2-8 into the Cl concentration versus depth profile shown in Figure 2-11.

The possibility that the SIMS analysis might distort the profile to be measured has been a concern (31). Figure 2-12 compares the SIMS profile of the implanted Cl in the oxide and the calculated distribution (34). There is no indication of severe

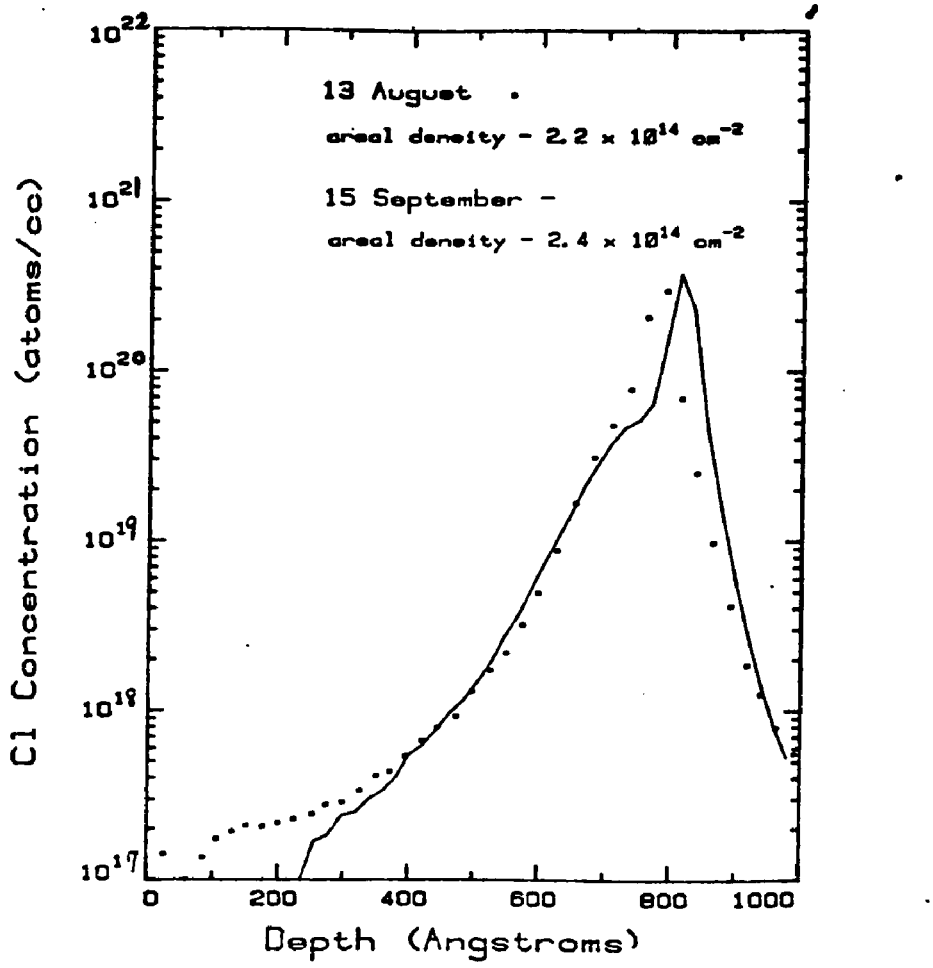

Fig. 2-10 The reproducibility of the RCA SIMS instrument.

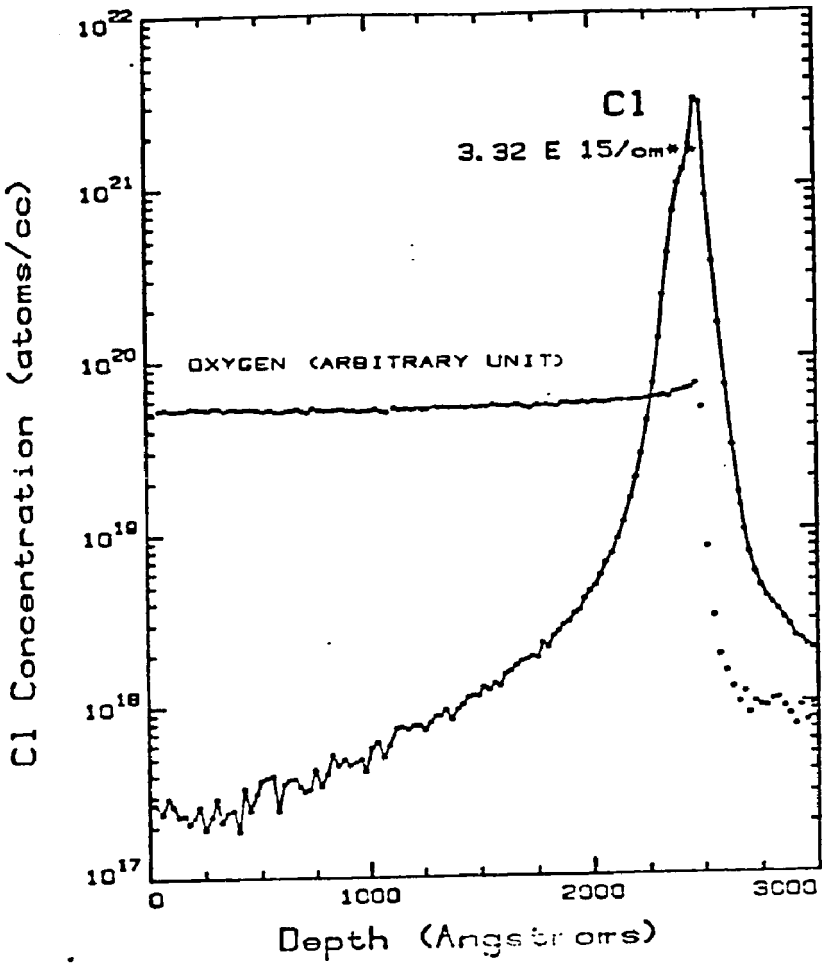

Fig. 2-11 The plot of the data converted from Fig. 2-8.

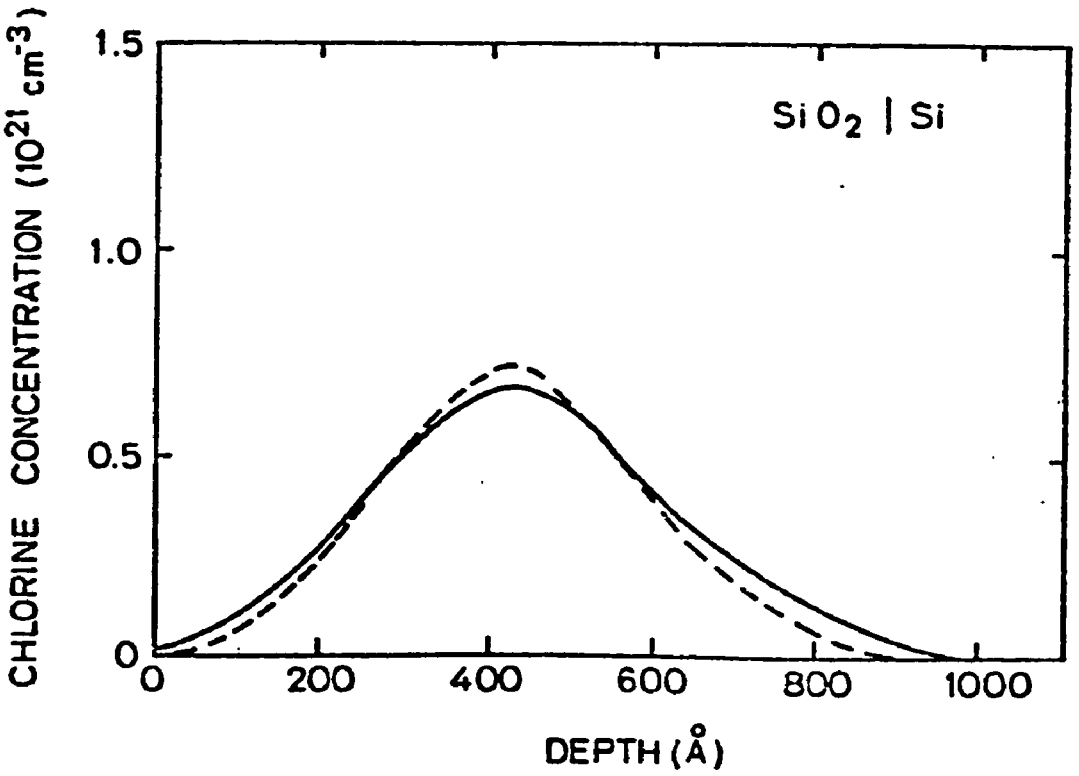

Fig. 2-12 SIMS profile of the implanted Cl in SiO_2. Dashed curve is the calculated Cl distribution (after Rouse, ref. 34).

distortion implying that Cl migration due to the SIMS measurement is not significant.

Hydrogen signals were also measured on some of the samples. See Fig. 2-2(d). These measurements were calibrated using implanted standards from a related study (30,35). Since these standards were not measured with the samples being analyzed for Cl, a somewhat larger uncertainty of the order of 200% was assigned to the absolute concentrations.

Chapter 3

Discussion and Modeling

3.1 Annealing of the Bonded Cl

3.1.1 Bonded Cl

To determine whether the implanted Cl is actually bonded in the network or remains interstitial and free to migrate, we start by considering the resulting profile of the implanted Cl shown in Fig. 2-4(a) after the reoxidation treatment (i.e. 20 minutes at 900°C). To begin, we assume the resultant profiles can be approximated by a gaussian function (38,39):

$$n(x,t) = \frac{\phi}{\sqrt{2\pi}\sqrt{\Delta R_p^2+2Dt}} \exp \frac{-(x-R_p)^2}{2(\Delta R_p^2+2Dt)} \qquad (3\text{-}1)$$

where ϕ is the dose,

R_p is the projected range

ΔR_p is the standard deviation of the projected range

$[2(D^*t)^{1/2}]$ is the diffusion length for the reoxidation treatment.

The diffusion length calculated for the reoxidation treatment is of the order of 1 μm, using a value of $D = 10^{-10}$ cm^2/sec for mobile Cl in bulk SiO_2 glass (40). Such a value should result in a flat profile with concentration of the order of $10^{16}/cm^3$ in Figure 2-4.

This is not what is observed.

For the case of the Cl incorporated during the thermal oxidation of Si, we also assume that the redistribution can be roughly approximated by a gaussian function inside the oxide:

$$C(x,t) = Q/(\pi Dt)^{1/2}\exp(-X^2/4Dt) \qquad (3\text{-}2)$$

where Q is the areal density of Cl at the Si/SiO_2 interface. For the same heat treatment (900°C for 20 minutes), the diffusion length of 1μm would result in a nearly flat profile with less than 10% variation in concentration across the oxide film. This is also not what is found (see Fig. 2-5). Therefore we recognize that the implanted Cl as well as the Cl incorporated during the thermal oxidation can not be mobile, molecular Cl; it is reacted Cl bonded into the SiO_2 network. This conclusion is in accord with studies of Al and O implantation in SiO_2 films (19,41).

Furthermore, Doremus observed that the concentration of the molecularly dissolved, mobile gas species in silicate glasses is about 1% of the gas-phase concentration (42). For 2% HCl in O_2 at 1100°C, we expect a value on the order of $10^{14}cm^{-3}$ for HCl. This is well below the detectability limit of the SIMS measurement. The observed Cl concentration in Figure

2-2 is much higher than this value, again implying that this Cl profile is that of reacted, immobile Cl bonded into the network (≡Si-Cl), and not molecular dissolved, mobile Cl.

As a summary, we recognize that both the Cl incorporated during thermal oxidation and the implanted Cl are reacted Cl, bonded into the SiO_2 network, not mobile molecular Cl.

3.1.2 Reaction-controlled Process

The redistribution of implanted ^{18}O in SiO_2 during the heat treatment in various H_2O-containing ambients was found to be a diffusion-controlled process in Pfeffer's study (19). However, it is not the conventional diffusion process; the oxygen diffusivity is found to be linearly proportional to the partial pressure of H_2O. It indicates the redistribution involves the exchange of H_2O with the network oxygen via the chemical reaction:

$$H_2{}^{16}O + -Si-{}^{18}O-Si- = -Si{}^{16}OH + -Si{}^{18}OH = H_2{}^{18}O + -Si-{}^{16}O-Si-$$

and the diffusion of the released H_2O. The chemical reaction is rapid enough that chemical equilibrium is attained and the overall rate of the process is determined by the slower diffusion process.

For the redistribution of the implanted Cl (or, in a broader sense, the bonded Cl) in water containing ambients, the question to be addressed is whether this process is diffusion or reaction-controlled. To begin, we assume that the conclusions of Pfeffer's study can be applied to the case of implanted Cl in SiO_2, i.e. (a) the redistribution of the implanted Cl in water containing ambients is a diffusion-controlled process; (b) the diffusivity of the implanted Cl is linearly proportional to the H_2O concentration. Also we assume the resultant profile can be described by the gaussian function in eq. [3-1], then the peak concentration of the implanted Cl can be simply expressed as

$$\frac{\phi}{\sqrt{2\pi}\ \sqrt{2Dt}}$$

considering ΔR_p^2 is negligible compared with 2 Dt. Therefore, this peak value should be inversely proportional to the square root of diffusivity, or the square root of the H_2O concentration in the annealing ambient. Unfortunately, the concentration range of the implanted Cl in this study and the sensitivity of the instrument did not allow us to draw any conclusion. For example, consider the data shown in Fig. 2-4. As the annealing ambient changes from 2 ppm to 2% H_2O, the peak concentration should drop by a factor of 100, i.e. from $2x10^{18}$ to $2x10^{16}$ which is below the detectability limit of

measurement. To get around this difficulty, let us now consider the data for Cl incorporated during the thermal oxidation of Si shown in Figure 2-5, instead of the implanted Cl. If we assume the redistribution of the Cl is also a diffusion-controlled process, the interfacial Cl concentration will be $\frac{\phi}{\sqrt{\pi Dt}}$ according to eq. 3-2. This value should decrease by a factor of 7 (i.e. the square root of 50) as the anneal ambients vary from 2% H_2O to wet O_2. However, as the results in Figure 2-5(c) show, the actual reduction was by far larger than the prediction based on the validity of diffusion-controlled process. Therefore we can conclude that the redistribution of the bonded Cl in H_2O-containing ambients is not a diffusion-controlled process. The interpretation of these data in terms of reaction-controlled processes will be discussed in detail later.

With this in mind, the results shown in Figure 2-4, can be interpreted as follows: during the reoxidation, the bonded Cl was released from the SiO_2 network, this mobile Cl diffused through the oxide, and was either incorporated into the new SiO_2 at the Si/SiO_2 interface (as evidenced by the pronounced peak) or escaped at the oxide/gas interface. We also note a small amount of Cl being directly incorporated into the film as the mobile species diffuse toward the interfaces. The overall redistribution is a reaction-controlled process. In the

slow replacement of Cl by O_2 in the dry O_2 case shows very little redistribution. However, in the 2% H_2O/O_2 ambient the water releases the Cl from the network and the high diffusion rate results in complete removal of the original implanted Cl. For the wet O_2 reoxidation, the complete removal of Cl from the new growing oxide shows that the interfacial incorporation reaction can also be suppressed by a high concentration of H_2O. These observations will be the basis for the modeling of the incorporation processes.

3.2 Modeling the Cl Incorporation in HCl Oxidation

In Figure 2-2(a), it is observed that at a position fixed with respect to the outer interface, the Cl concentration decreases as oxidation proceeds beyond that point. In order for this to occur, there must be some "replacement reaction" such as:

$$-\underset{|}{\overset{|}{Si}}- Cl + H_2O = -\underset{|}{\overset{|}{Si}}-OH + HCl \qquad (a)$$

to release the bonded Cl from the network, thereby decreasing the Cl concentration. Such a reaction is supported by independent evidence (23,24). The Cl released in the bulk oxide would diffuse to the interface where it would react again resulting in a net accumulation process. The overall Cl incorporation processes can now be summarized as follows: during the oxidation, the Cl molecular species dissolve at the outer interface, dif-

fuse to the Si/SiO_2 interface, react with the Si and become part of the oxide network. Some of this incorporated Cl subsequently reacts with the diffusing H_2O and is replaced by OH. This occurs because the local thermodynamic conditions change as the interface moves on during the continuing oxidation process.

We begin the modeling of the Cl replacement reaction by considering the concentration profile of the diffusing mobile species in the oxide, see Figure 3-1. According to the steady state oxidation model of Deal and Grove (23), when the oxide thickness is $X_o(t)$, these concentrations are given by:

$$C_{ox}(x) = C^o_{ox}\left(1 - \frac{x}{x_o+A/2}\right) \qquad (1)$$

$$C^{HCl}(x) = C^o_{HCl}\left(1 - \frac{x}{x_o+A'/2}\right) \qquad (2)$$

$$C_w(x) = C^o_w \left(1 - \frac{x}{x_o+A''/2}\right) \qquad (3)$$

where C_{ox}, C_{HCl}, C_w are the O_2, HCl, and H_2O concentrations, respectively. C^o_{ox}, C^o_{HCl}, C^o_w are the concentration of these species at the outer interface. A, A' and A'' are the ratio of the diffusivity to the reaction rate constant at the Si/SiO_2 interface for O_2, HCl and H_2O, respectively. For the immobile species Si-OH, the concentration is approximately constant:

$$C_{Si-OH} = C_{OH} = \text{measured H concentration} \qquad (4)$$

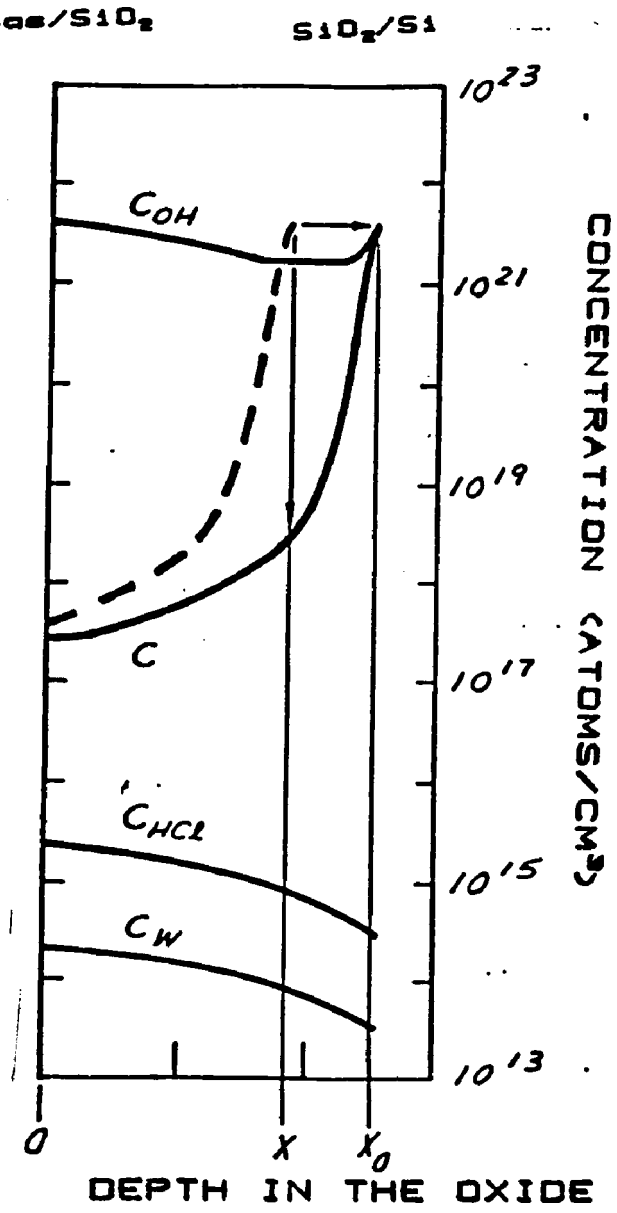

Fig. 3-1 Schematic concentration profiles for Cl, SiOH, HCl and H_2O in an oxide of thickness X_o. The dashed profile represents the Cl concentration profile when the Si/SiO_2 interface was at position X.

As a first approximation we take A = A' = A". The kinetic equation for the replacement reaction given in eq. (a) can be written as:

$$\frac{dC}{dt} = - k_1 \, C \, C_w + k_2 \, C_{OH} \, C_{HCl} \qquad (5)$$

where C is the concentration of bonded Cl, k_1 and k_2 are the reaction rate constants for the forward and reverse reaction. C_{OH} is the concentration of SiOH. Since we are investigating the reaction during the oxidation process, the differential with respect to time can be converted to one with oxide thickness (11),

$$dt = (X_o + A/2)(2/B)dx_o \qquad (6)$$

B is the parabolic rate constant. We then substitute equations 2, 3, and 4 into equation 5 and set up the integral using eq. (6):

$$\int_{C_i k_d - k_i}^{C_f k_d - k_i} \frac{d(Ck_d - k_i)}{(Ck_d - k_i)} = - k_d \int_{x_o = x}^{x_o = x_f} (2x_o + A - 2x)dx_o \qquad (7)$$

where

$$K_d = \frac{C_w^o K_1}{B} \qquad (8)$$

$$K_i = \frac{C_{OH}^o \, C_{HCl}^o \, K_2}{B} \qquad (9)$$

We remind the reader that this integration is at a

position x in the oxide and thus C_i is the Cl concentration at the Si/SiO_2 interface when it is at the position x. Correspondingly, C_f is the Cl concentration at the position x when the oxide is grown to the final thickness x_f. The integration result can be expressed as:

$$\ln\left(\frac{C_f-C_o}{C_i-C_o}\right) = -k_d[(x_f-x)^2 + A(x_f-x)] \qquad (10)$$

It can be readily shown that $K_i/K_d = C_o$, and C_o is the equilibrium concentration of Si-Cl at the outer interface. To facilitate the analysis we let

$$(x_f - x)^2 + A(x_f - x) = \{x'\}^2. \qquad (11)$$

To a good approximation, C_o can be neglected when compared to C_f and C_i. The final form of the expression is:

$$\ln C_f = -k_d(x')^2 + \ln C_i \qquad (12)$$

where $k_d = k_i C_w/B$

On a plot of log C_f versus $\{x'\}^2$ eq. 12 is a linear equation with slope and intercept equal to k_d and log (C_i), respectively. Figure 3-2 is such a replot of the original data. In the region close to the Si/SiO_2 interface, the data can be fit by a straight line.

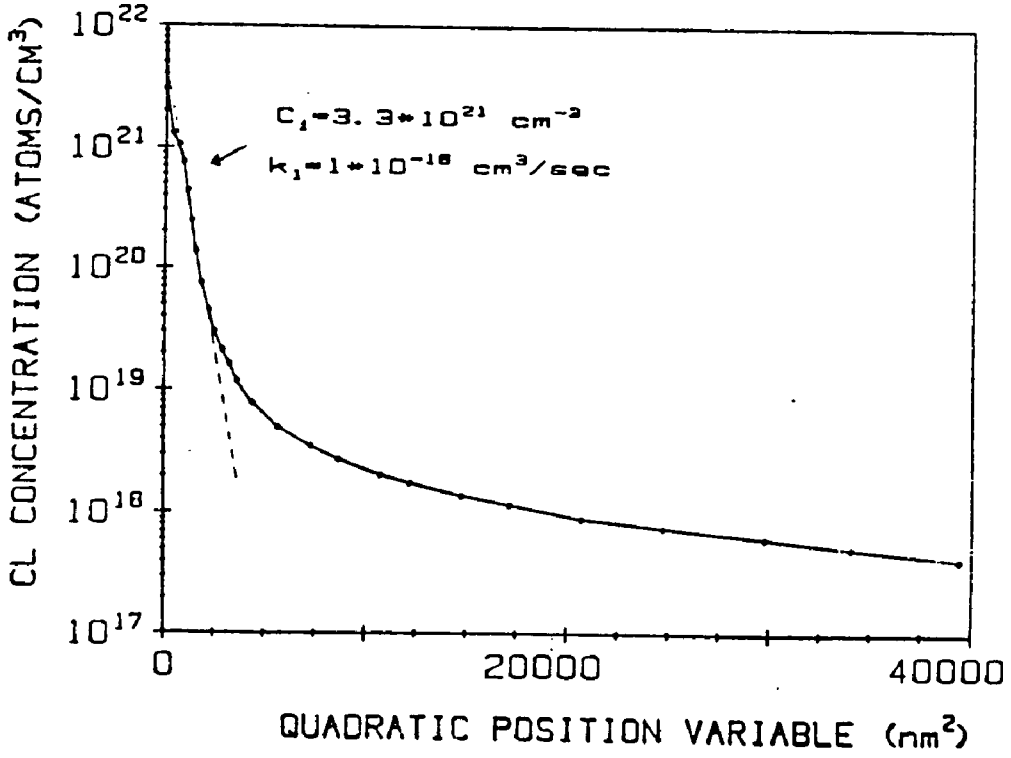

Fig. 3-2 Replot of the data in Figs. 2-2(a) for an HCl/O_2 oxidation of 160 minutes. These data are plotted according to the relationship of eq. (12). The abscissa is the quadratic position variable defined in eq. (11).

However, in the region farther away from the interface, the concentration does not decrease as rapidly as predicted by this line. We interpret this to show that there are Cl species in the network (with smaller concentrations) that can not be readily replaced by OH. Figure 3-3(a-f) shows the Cl versus depth profiles can be fit by two or three such exponential functions with appropriate values of the slope and intercept as listed in Table 3-1. The fitting procedure is as follows: First, the lower concentration region in the replot of the data shown in Fig. 3-2 is fitted with a linear function. Then this linear function is extrapolated into the higher concentration region and subtracted from it. The subtracted data is again fitted by a linear function. The overall fitted function is the sum of these linear functions. At the present time we do not have an interpretation of these other "branches" of the fit. It is noteworthy that the implanted Group III elements (Ga, In, and Tl) and Group V element (As) in SiO_2 were found to occur in several chemical states (44,45,46). Additionally, the reaction whereby O_2 replaces Cl has been demonstrated in the annealing experiment with implanted Cl in Figure 2-4. Therefore it seems to be a reasonable speculation that these other "branches" can be attributed to the different chemical states of the bonded Cl

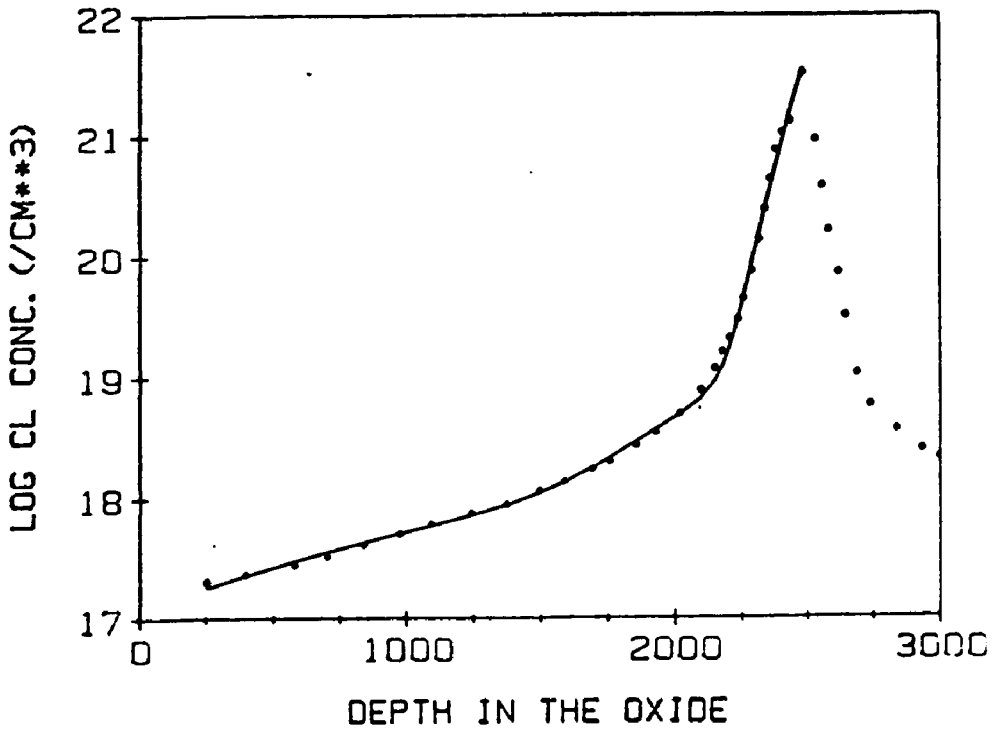

Fig. 3-3(a) A comparison of the fit of the model (solid line) and the data (points) for oxide grown in composition A for 160 minutes.

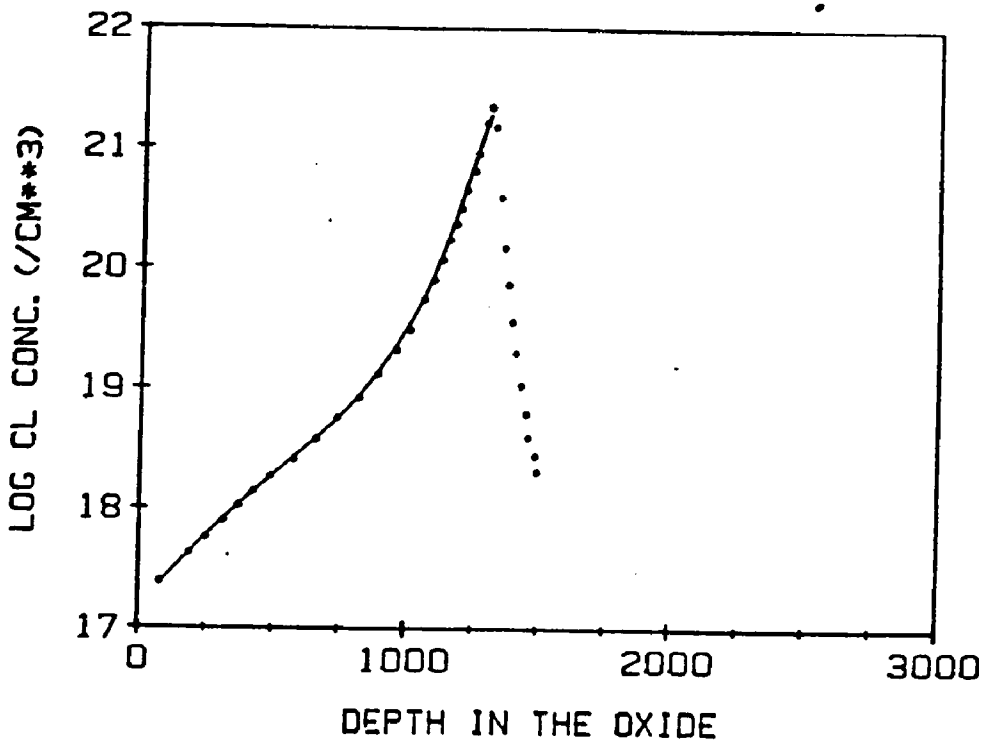

Fig. 3-3(b) A comparison of the fit of the model (solid line) and the data (points) for oxide grown in composition A for 40 minutes.

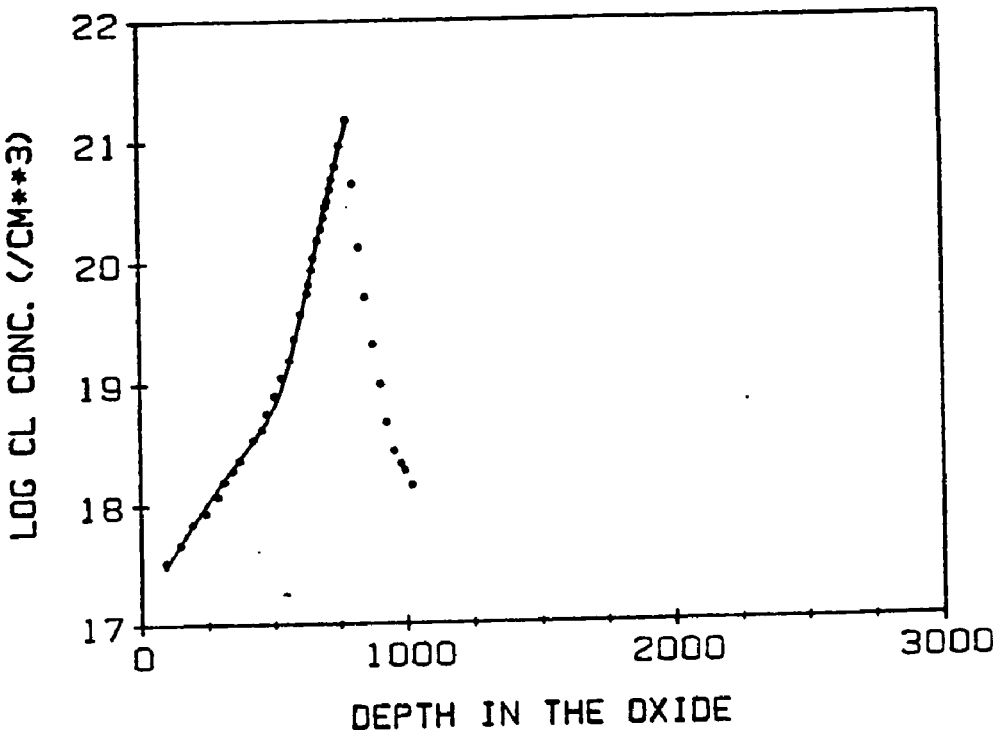

Fig. 3-3(c) A comparison of the fit of the model (solid line) and the data (points) for oxide grown in composition A for 20 minutes.

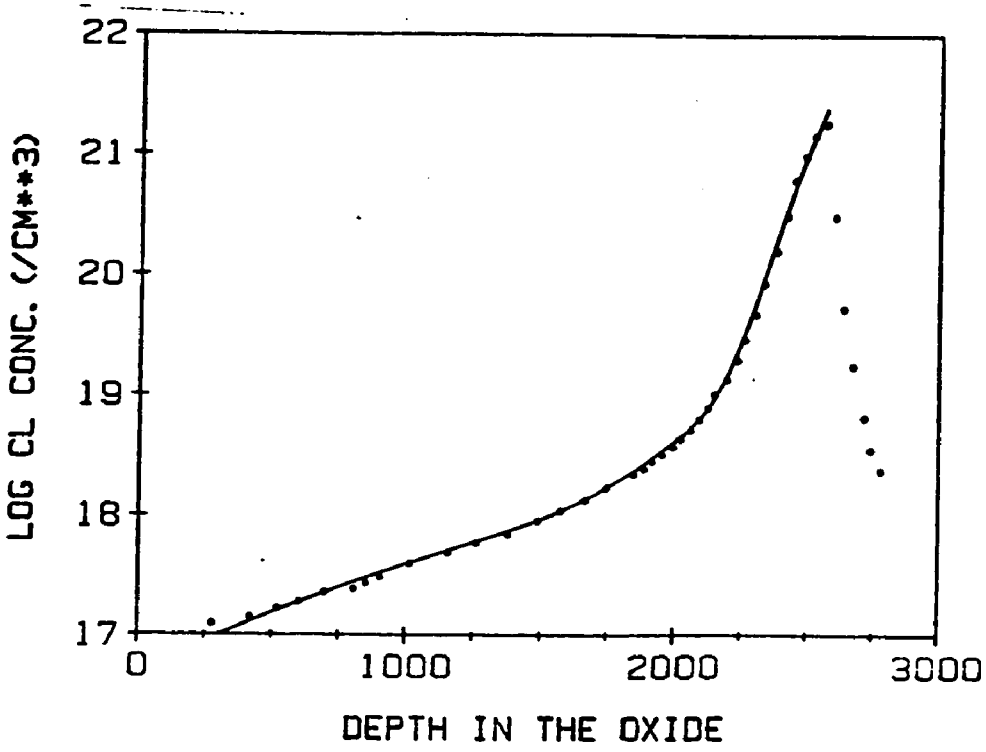

Fig. 3-3(d) A comparison of the fit of the model (solid line) and the data (points) for oxide grown in composition D for 160 minutes.

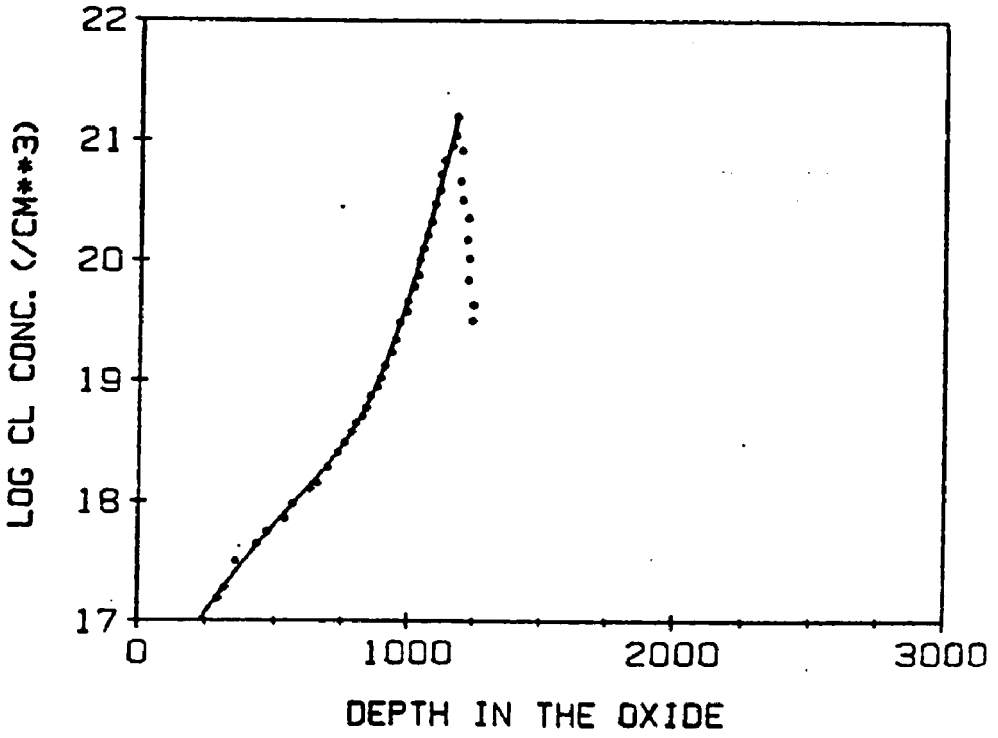

Fig. 3-3(e) A comparison of the fit of the model (solid line) and the data (points) for oxide grown in composition D for 40 minutes.

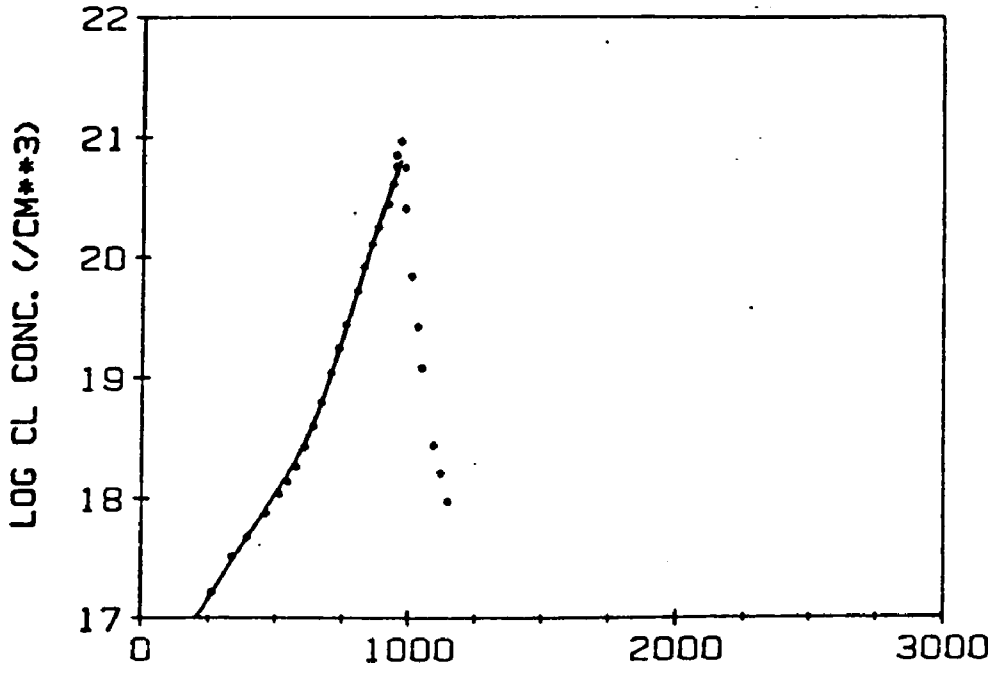

Fig. 3-3(f) A comparison of the fit of the model (solid line) and the data (points) for oxide grown in composition D for 20 minutes.

Table 3-1

$C(1/cm^3)$ and $k(cm^3/sec)$ values for fitting the model to the data involving two or three exponential functions: $C = C_1 \exp(-k_1 x) + C_2 \exp(-k_2 x) + C_3 \exp(-k_3 x)$.

Sample	C_1	k_1	C_2	k_2	C_3	k_3
2% HCl, 20 min	1.35×10^{21}	1.17×10^{-16}	1.58×10^{19}	1.97×10^{-17}		
2% HCl, 40 min	1.66×10^{21}	1.04×10^{-16}	2.24×10^{20}	3.75×10^{-17}	1.78×10^{19}	8.88×10^{-18}
2% HCl, 160 min	3.55×10^{21}	1.02×10^{-16}	1.41×10^{19}	1.18×10^{-17}	1.51×10^{18}	1.56×10^{-18}
1% HCl, 20 min	6.17×10^{20}	1.27×10^{-16}	1.20×10^{19}	3.34×10^{-17}		
1% HCl, 40 min	1.07×10^{21}	2.13×10^{-16}	3.47×10^{20}	1.03×10^{-16}	1.17×10^{19}	2.39×10^{-17}
1% HCl, 160 min	2.24×10^{21}	1.10×10^{-16}	2.19×10^{19}	2.25×10^{-17}	2.00×10^{18}	3.76×10^{-18}

or other replacement reactions.

In Table 3-2 we summarize the results of fitting the data in the region near the Si/SiO_2 interface using A and B values from (27) for six different sets of oxidation conditions. We see that the k_1 values are reasonably independent of time and HCl concentration as the model requires. There is a small dependence of C_i on time that we did not consider. However, the increase of C_i with HCl concentration is in qualitative agreement with the model. Therefore it appears that the shape of the Cl concentration versus depth profile in the high concentration range near the interface is determined by the kinetics of the replacement reaction.

The Cl concentration profiles for the oxides grown in 2% HCl at 1200°C is shown in Appendix IV. A plateau on the Cl concentration profile near the Si/SiO_2 interface was observed. Also the total Cl is higher than $2x10^{15}/cm^2$, and therefore the Cl-rich third phase may be present. This phase is known to be easily etched and therefore could cause non-uniform sputtering and degrade the depth resolution. Due to the possible complication of this third phase, the simple model derived here can not be applied to the 1200°C data to obtain the activation energy for the kinetic rate constant of the replacement reaction.

Table 3-2

Summary of the Fitting Results in the Region

Near the Si/SiO_2 Interface

	1% HCl		2% HCl	
Time (min)	$k_1(cm^3/sec)$	$C_i(1/cm^3)$	$k_1(cm^3/sec)$	$C_i(1/cm^3)$
20	$1.2x10^{-16}$	$6.46x10^{20}$	$1.1x10^{-16}$	$1.32x10^{21}$
40	$1.5x10^{-16}$	$1.29x10^{21}$	$0.8x10^{-16}$	$2.09x10^{21}$
160	$1.0x10^{-16}$	$2.09x10^{21}$	$1.0x10^{-16}$	$3.31x10^{21}$

3.3 Cl_2 Type Oxidation

As discussed above, the interfacial Cl concentration is determined by the active Cl molecular species which dissolve at the outer surface and diffuse to the Si/SiO_2 interface where they are incorporated. Detailed comparison of plots like Figure 2-2(a) and 2-2(b) shows that the interfacial Cl concentration in HCl type oxides is always higher than that in Cl_2 type oxides. Figure 2-2(c) is an example of this comparison. Since these two oxides were prepared with the same Cl_2 partial pressure, as table 2.1 shows, this observation indicates that both HCl and Cl_2 contribute to the interfacial incorporation process.

Moreover, Figure 2-2(c) shows Cl was more broadly distributed in the region near the Si/SiO_2 interface for the Cl_2 oxide. Rutherford backscattering spectrometry (RBS) also shows that the Cl is more uniformly distributed in the Cl_2 oxides than in the HCl oxide (6). We do not have a detailed model to explain the Cl depth profile in the Cl_2 oxide as we do for the HCl case. However, as discussed in the modeling section, we know the rate at which the Cl concentration decreases with distance from the interface is related to the kinetics of the "replacement" reaction, and therefore this "rate" is significantly slower in the Cl_2 oxides. Since in the

case of Cl_2 oxide, oxygen is the predominant species available to replace the bonded Cl, the shape difference implies that the oxygen replaces the bonded Cl at a slower rate than H_2O does in the HCl oxide. This conclusion is consistent with the observation in the annealing experiment of the implanted Cl as shown in Figure 2-4.

Additionally, by analogy with the previous model, the following reaction involving the replacement of the bonded chlorine by oxygen can be obtained:

$$-Si-Cl..Cl-Si- + O_2 = -Si-O-O-Si- + Cl_2 \qquad (b)$$

where -Si-O-O-Si- is the "peroxy-radical" (32). The concentration of this species is of the order of $10^{20}/cm^3$ in bulk SiO_2 according to a recent paper based on thermodynamic considerations (54). Following a similar analysis procedure with this reaction as that applied to Eq. (a), a reaction rate constant of the order of 10^{-20} cm^3/sec was obtained from the slope of the straight line in the region near the Si/SiO_2 interface as shown in Fig. 3-4. Comparing this value with that of the HCl oxide (i.e. $10^{-16}cm^3/sec$), we can see how the shape change in the Cl concentration profile near the Si/SiO_2 interface was reflected in the change of the kinetic rate constant. These values will be discussed later.

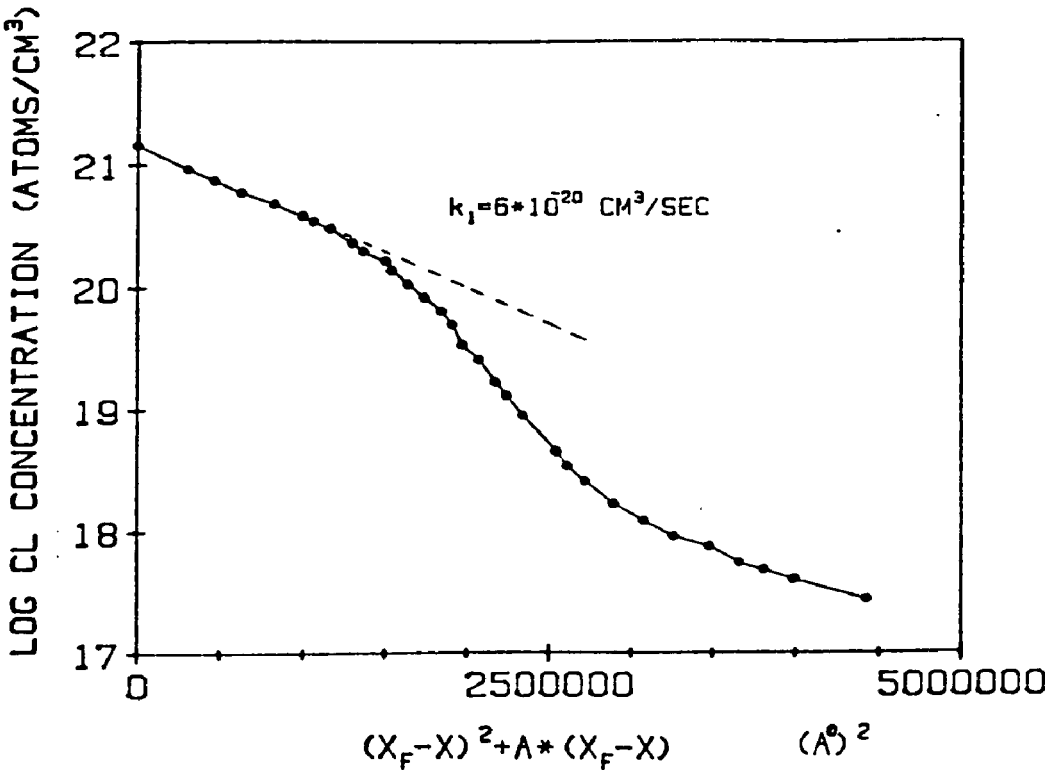

Fig. 3.4 Replot of the data in Fig. 2.2(b) for a Cl_2/O_2 oxidation for 40 min. These data are plotted according to the relationship of eq. (12). The abscissa is the quadratic position variable defined in eq. (11).

We briefly comment on the "field-aided diffusion" model proposed to explain the Cl depth profiles (11). In this model, the Cl was driven through the oxide by an electrochemical field to a chemical potential sink, i.e. the Si/SiO_2 interface. Then the flux of Cl can be expressed as

$$J = -D \frac{\partial C}{\partial x} + \mu F C$$

where J is the flux of Cl

D is the diffusivity of Cl

$\frac{\partial C}{\partial x}$ is the concentration gradient of Cl

μ is the mobility of Cl, and

F is the electrochemical field inside the oxide. With steady state approximation, this differential equation can be solved:

$$C_{(x)} = C_1 + C_2 \exp(bx)$$

where b is a constant related to the electrochemical field. This is an exponentially increasing function as shown in Fig. 3-5(a). Auger sputter profiling (ASP) was used to measure the Cl concentration at the Si/SiO_2 as shown in Fig. 3-5(b). Therefore, the overall Cl profile can be described by an exponentially increasing function in the bulk SiO_2 and a delta function at Si/SiO_2 interface where the Cl accumulates. See Figs. 3-5(a) and (b). However, as Fig. 3-5(c) shows, a

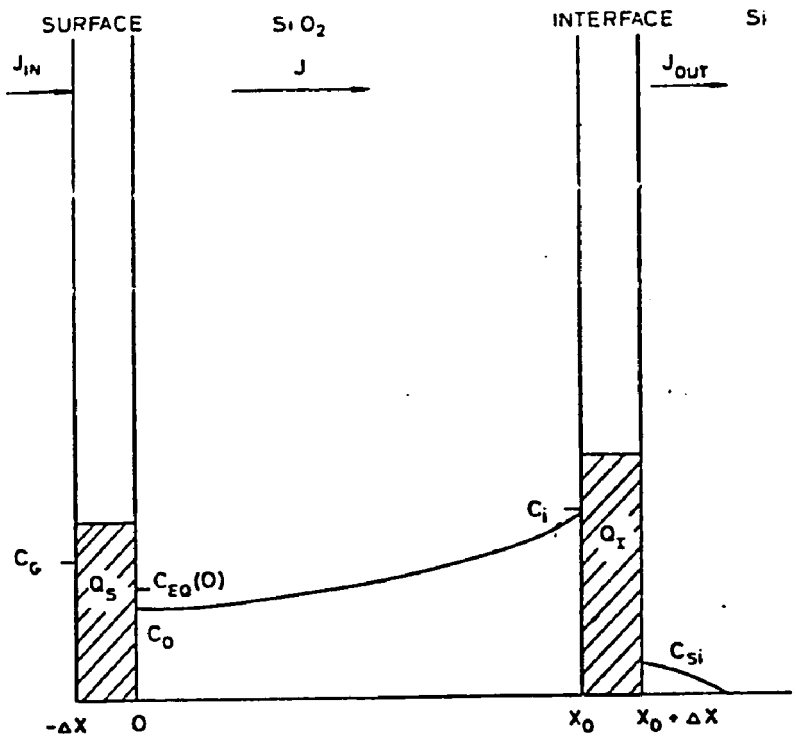

Fig. 3.5(a) Schematic illustration of the SiO_2/Si structure during particle transport. The surface, bulk, and interface regions are each characterized by distinct structural properties. Particle accumulation in the surface and interface is denoted by $Q(cm^{-2})$. Also shown are the various flux terms. The important concentration levels are C_G (gas phase concentration), $C_{EQ}(0)$ (equilibrium concentration in SiO_2 at x=0), C_O (actual concentration in SiO_2 at x=0), C_i (concentration in SiO_2 at $x=x_o$), and C_{Si} (concentration in silicon substrate at $x=x_o + \Delta x$). (Reproduced from Rouse, ref. 34).

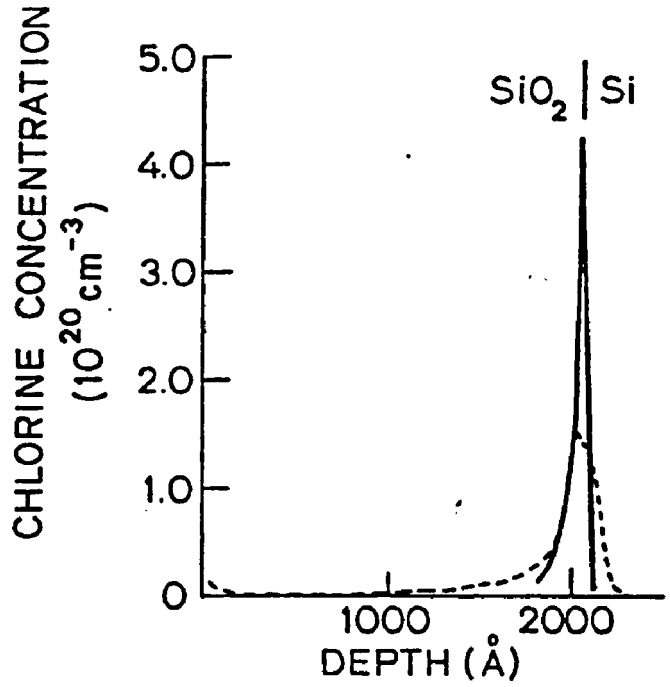

Fig. 3.5(b) Chlorine distribution as a function of depth for SiO_2 grown in O_2/5% HCl at 1100°C. Linear plot, where the solid curve is the Auger sputter profile. The profile cuts off at the sensitivity limit for this measurement technique. The dashed curve is the SIMS profile for the same sample. (Reproduced from Rouse, ref. 34)

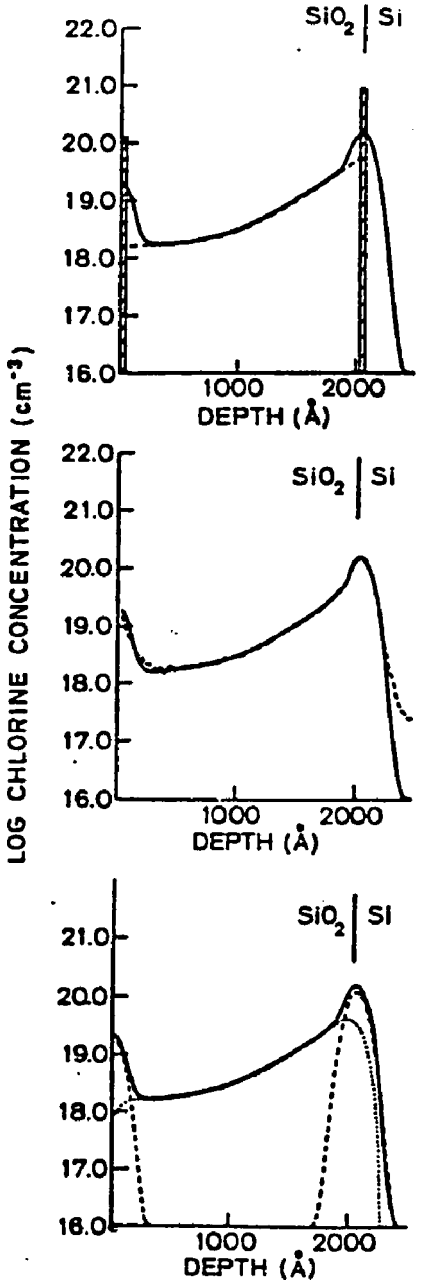

Fig. 3.5(c) Development of the analytical expression for the chlorine distribution including broadening effects. This expression is indicated in each panel by the solid curve. (I) The original chlorine distribution is modeled by a surface peak, interface peak, and bulk oxide distribution (dashed curve) given by $C_1+C_2 \exp(bx)$. (II) The dashed curve is the actual SIMS data for SiO_2 grown in O_2/5% HCl at 1000°C. (III) Components of (I) after broadening with a Gaussian having a 170 Å FWHM. (Reproduced from Rouse ref. 34)

gaussian shape Cl profile was observed in the region near the Si/SiO_2 interface in their SIMS data. The discrepancy was attributed to the "broadening" or "knocking on" effect of the primary ion beam in the SIMS measurement (11,34). According to this argument, the shape of Cl profile in this region should be the same in a HCl or Cl_2 oxide if the same primary beam is used in the SIMS measurements. Thus the differences shown in Figure 2-2(c) demonstrate that this can not be the explanation of the profiles determined with our instrument, while our model based on the kinetics of the "replacement reaction" explains this shape difference. Furthermore, if such a field exists in the oxide, it is conceivable that this field should similarly affect the in-diffusing species during the oxidation. Therefore, similar concentration vs. depth profile in the bulk SiO_2 is expected for these in-diffusing species. However, the fluorine profile in the fluorinated oxide as shown in Fig. 3-6, which will be discussed in detail later, shows this is not the case. For oxygen, profiling analysis of oxides with a short additional growth in $^{18}O_2$ (20) shows the shape of ^{18}O concentration profile in the bulk SiO_2 approximately follows that in Fig. 3-1. This again contradicts the prediction based on the "field-aided diffusion" model. Moreover, the "field-aided diffusion" model

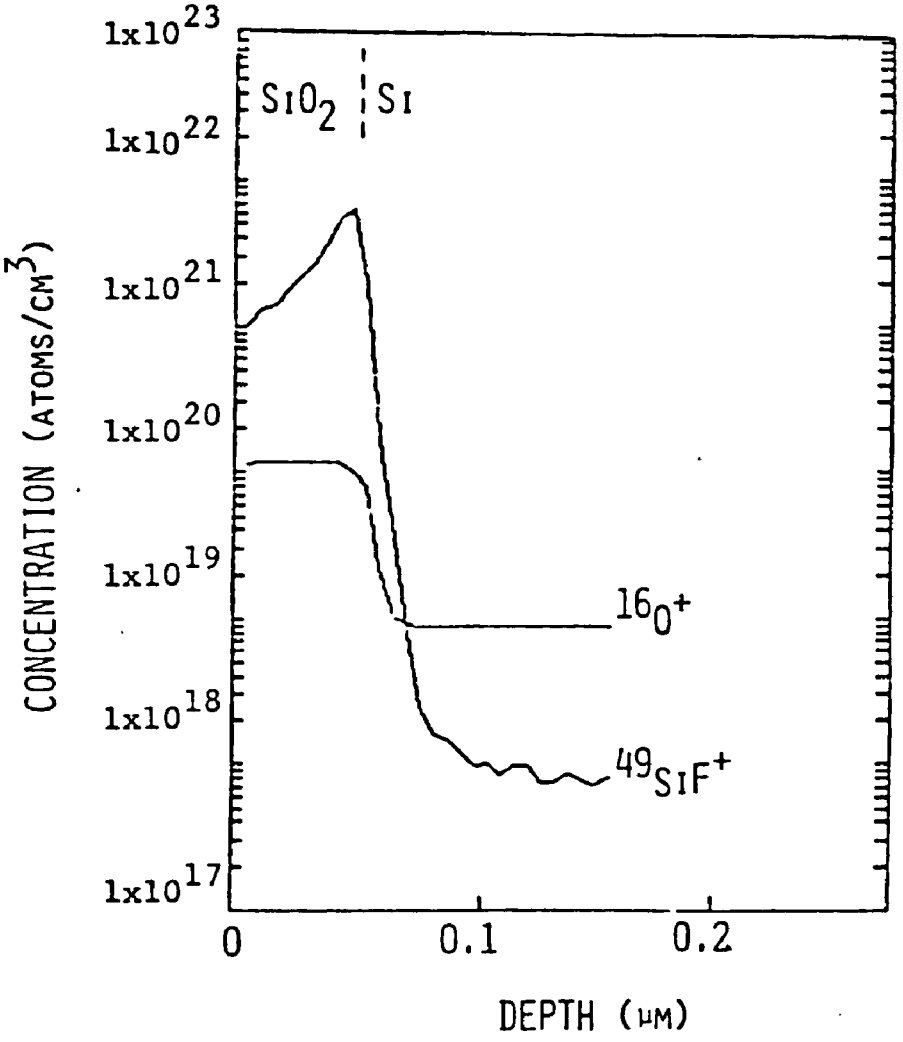

Fig. 3-6(a) Fluorine and oxygen profiles of an oxide grown for 1 hour at 900°C with 0.011 vol% $C_2H_3Cl_2F$ in O_2 (reproduced from Wolowodiuk, ref. 47).

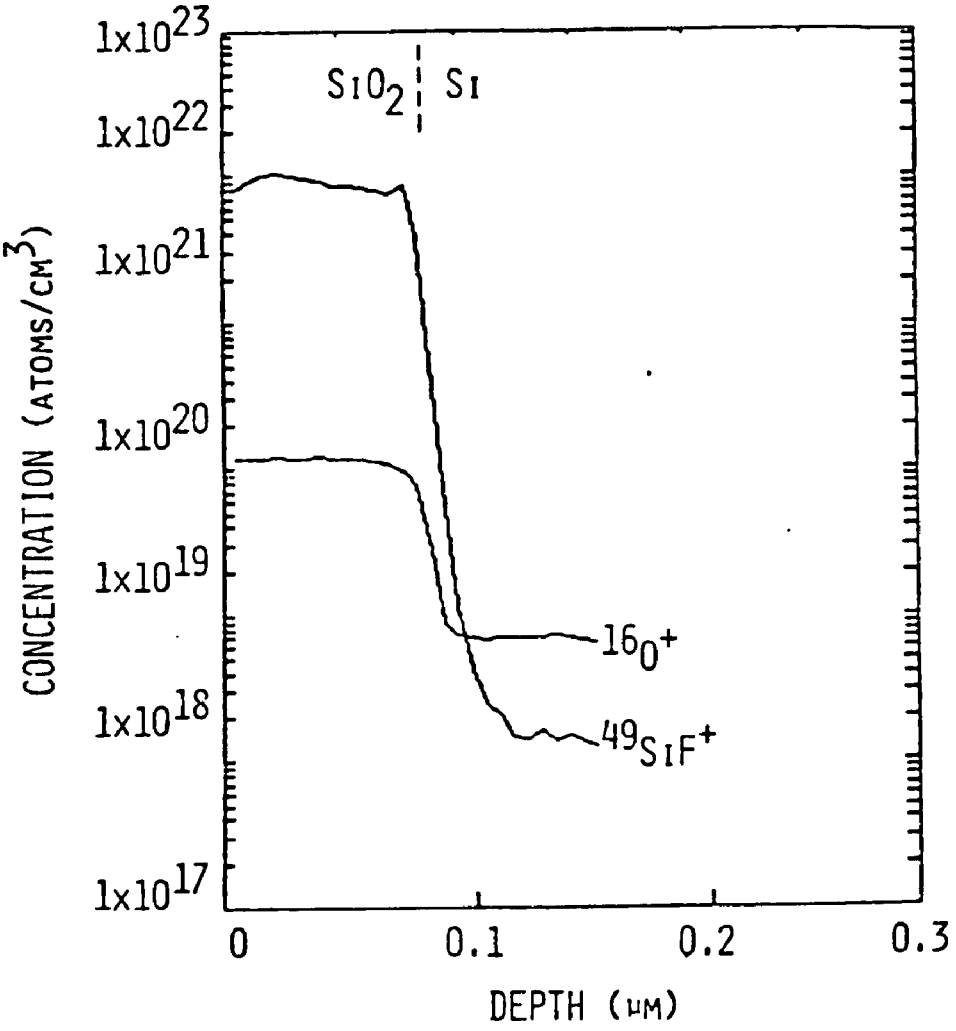

Fig. 3-6(b) Fluorine and oxygen profiles of an oxide grown for 2 hours at 900°C with 0.011 vol% NF_3 in O_2 (reproduced from Wolowodiuk, ref. 47).

would imply different functional forms other than eqs. (1), (2), (3) for the concentration profiles of the in-diffusing species. Since these equations fit directly into our model, any such change as implied by the "field-aided diffusion" model is inconsistent with the agreement between our model and the data.

3.4 Comparison with Related Studies

Wolowodiuk recently studied the addition of fluorine to the oxidation ambient in "wet" ($C_2H_3Cl_2F/O_2$) or "dry" (NF_3/O_2) atmospheres (47). Typical fluorine concentration versus depth profiles are shown in Figure 3-6. It was observed that the profile of F in the "wet" fluorine oxide was similar to that of Cl in the HCl oxide; the F concentration peaked at the Si/SiO_2 interface and decreased into the bulk of SiO_2, while in the "dry" fluorine oxide the profile is fairly flat. These observations are generally in accord with the model proposed in this study. The apparent difference is that F is so stable in the oxide that oxygen does not replace it rapidly and therefore a flat profile is observed. In contrast, Cl is less stable in the oxide due to the smaller electronegativity, and can be replaced by the oxygen as discussed above. However, both Cl and F can be replaced by OH which results in a peaked profile. This is also consistent with recent work on OH removal

from optical fibers preforms by the use of fluorine-containing compounds (48).

Rouse et al. (11) examined oxide grown in O_2/5%HCl and then annealed in Ar at 1100°C for 1 hour. No evidence of depletion of interfacial Cl was observed. However, when the sample was annealed in O_2, most of the Cl was found to be depleted from the interface. This observation is consistent with our observation that O_2 can replace the bonded Cl. It also indicates that some anion must be present to replace the Cl if it is to be released from the network. They also studied the kinetics of the exchange of the oxygen in SiO_2 during thermal oxidation in dry O_2 (20). The reaction rate constant was estimated to be 10^{-22} cm^3/sec at 1150°C. Oxygen, being one of the major constituents in SiO_2, is far more stable than Cl. Therefore, the larger kinetic rate constants ($10^{-16}cm^3$/sec and $10^{-20}cm^3$/sec at 1100°C for Cl replacement by H_2O and O_2, respectively) obtained in this study seem to be reasonable.

3.5 HCl Type Oxidation

In Figure 2-3(a) we see the increase in the total Cl with Cl_2 partial pressure. This is the expected result if Cl_2 is the active species driving an incorporation reaction. However, in Figure 2-3(b) the opposite trend is found with increasing HCl partial

pressure. This appears to contradict the earlier suggestion that both HCl and Cl_2 are active species driving incorporation reactions. We believe that both HCl and Cl_2 are active and that the difference obtained here is due to the large increase in H_2O partial pressure required to keep the Cl_2 partial pressure constant. To understand this we note that during the oxidation in HCl/O_2 ambients incorporation processes occur at the Si/SiO_2 interface that can be formally represented by the following reactions:

$$Si + HCl = Si\text{-}Cl + 1/2\ H_2 \qquad (13)$$

$$Si + Cl_2 = Si\text{-}Cl + 1/2\ Cl_2 \qquad (14)$$

$$2Si + O_2 = Si\text{-}O\text{-}Si + 1/2\ O_2 \qquad (15)$$

$$2Si + H_2O = Si\text{-}O\text{-}Si + H_2 \qquad (16)$$

The incorporation reactions in equations 13 and 14 should compete with the oxidation reactions in eqs. 15 and 16 for Si at the Si/SiO_2 interface. Therefore, as noted earlier, the Cl incorporation can be suppressed by increasing the H_2O in the oxidation ambient. Thus we see that H_2O plays a double role in HCl/O_2 oxidations, suppressing the Cl incorporation at the interface and replacing Cl in the "bulk" of the oxide.

In the above incorporation reactions, the chemical nature of the Si has not been specified. In trying to

understand this, the basic mechanisms of the oxidation of Si have to be considered. During the transformation of Si into SiO_2, a volume change per Si of 225% is required. Therefore a supply of "free volume" is needed at the Si/SiO_2 interface to sustain the oxidation. The "free volume" can be accommodated either by a flow of vacancies from the bulk Si, a flow of Si interstitial from the interface into the bulk Si and SiO_2, or a viscous flow in the oxide (49). Viscous flow has been experimentally observed during the thermal oxidation of Si (52,53). Also, oxidation induced stacking fault growth and oxidation enhanced diffusion are considered as evidences of the interstitial Si flow in bulk Si (50). A Si-rich region in SiO_2 with the width of 1nm or less near the Si/SiO_2 interface has been found (51). The interstitial generation model would imply this region is where most of the interstitials react with in-diffusing oxidants such as O, Cl, F, OH, etc.

The addition of HCl or TCA to the oxidation ambients suppressed the growth of oxidation induced stacking faults as mentioned in the first chapter. Lin et. al. suggested that Cl reacts with the interstitial Si near the Si/SiO_2 interface, which reduces the supersaturation of interstitial Si near the interface and thus suppressed the growth of oxidation induced

stacking faults (55). They speculated that the observed Cl pile-up at the Si/SiO_2 interface in the chlorinated oxide is also due to the same reaction. On the other hand, bond breaking at the Si/SiO_2 interface must occur to sustain the viscous flow during the oxidation. Therefore, it seems to be likely that the Cl reacts with these active Si which result from the interstitial formation of viscous flow, and thereby are incorporated at the Si/SiO_2 interface.

Chapter 4

Conclusions and Suggestions for Future Studies

The findings in this study are summarized as follows:

(1) Both the implanted Cl and the Cl incorporated during the thermal oxidation of Si are bonded into the network. Some anion must be present to replace the Cl if it is to be released from the network.

(2) For HCl oxides, the Cl profile as a function of oxidation time shows the Cl is replaced by OH. The shape of the Cl profile near the Si/SiO_2 interface can be quantitatively modeled by the kinetics of the replacement reaction.

(3) The interfacial Cl incorporation is controlled by both HCl and Cl_2 which react with the active Si near the Si/SiO_2 interface. This active Si presumably results from the oxidation process. H_2O interferes with these processes.

(4) For Cl_2 oxides, similar bulk replacement reactions also occur as with the HCl oxide, although at a slower rate, presumably by reacting with O_2.

The following are suggested as further experiments:

(1) Growing the HCl oxides at lower temperatures, e.g. 1000°C and 900°C. The oxides can be analyzed by SIMS to obtain the Cl concentration versus depth profile. The reaction rate constant can be obtained with

the procedure described in the modeling section. Then the activation energy for the replacement reaction can be deduced from the temperature dependence of the reaction rate constant. This value can be then compared with the activation energy for total Cl incorporated in ref. (12) in order to try to gain insight into the interfacial contribution to the overall incorporation.

(2) X-ray photoelectron spectroscopy (XPS) has been used to study the chemical state of the bonded Cl in highly chlorinated oxides (i.e. oxide grown in 10% HCl at 1100^{o}C for 1 hr) (56). Similar studies should be carried out on the oxide with lower Cl concentration to see if several chemical species can be identified.

References

1. L. E. Katz, in VLSI Technology, S. M. Sze editor, p. 131, McGraw-Hill, N.Y. (1983).

2. R. J. Kriegler, Y. C. Cheng and D. R. Colton, J. Electrochem. Soc. 119, 388 (1972).

3. H. Shiraki, J. Appl. Phys., 15, 1 (1976).

4. C. M. Osburn, J. Electrochem. Soc. 121, 809 (1974).

5. D. W. Hess and B. E. Deal, J. Electrochem. Soc. 124, 735 (1977).

6. Y. J. van der Meulen, C. M. Osburn, and J. F. Ziegler, J. Electrochem. Soc. 122, 284 (1975).

7. A. Rohatgi, S. R. Butler, F. J. Feigl, H. W. Kraner and K. W. Jones, J. Electrochem. Soc. 126, 143 (1979).

8. B. E. Deal, A. Hurrle and M. J. Schulz, J. Electrochem. Soc. 125, 2024 (1978).

9. M. D. Monkowski, J. R. Monkowski, I. S. T. Tsong, J. Stach, and R. E.. Tressler, J. Non-Crystalline Solid 49, 201 (1982).

10. H. Frenzel and P. Balk, J. Vac. Sci. Technol. 16, 1454 (1979).

11. J. W. Rouse, C. R. Helms, B. E. Deal, and R. R. Razouk, J. Electrochem. Soc. 131, 887 (1984).

12. W. A. Rosenberg, C. W. Magee, and E. A. Botnick, J. Electrochem Soc. 131, 2397 (1984).

13. H. L. Tsai, S. R. Butler, D. B. Williams, H. W. Kraner and K. W. Jones, J. Electrochem. Soc. 131, 411 (1984).

14. Y-D Sheu, S. R. Butler, F. J. Feigl and C. W. Magee, Abstract 237, p. 341, The Electrochemical Society Extended Abstracts, Vol. 85-1, Toronto, May 1985.

15. Y. J. van der Meulen and J. G. Cahill, J. Electronic Materials 3, 371 (1974).

16. J. Monkowski, R. E. Tressler, and J. Stach, J. Electrochem. Soc. 125, 1867 (1978).

17. J. Monkowski, J. Stach, and R. E. Tressler, Proc. 30th Electronic Eomponent Conf., San Francisco, CA (1980).

18. E. Rosencher, A. Straboni, S. Rigo and G. Amsel, Appl. Phys. Lett. 34, 255 (1979).

19. R. Pfeffer and M. Ohring, J. Appl. Phys. 52, 777 (1981).

20. J. W. Rouse, C. R. Helms, C. J. Han, Computer Aided Design of Integrated Circuit Fabrication Process for VLSI Devices, Final Report, Stanford, 1982.

21. T. H. Elmer, J. Am. Cer. Soc. 64, 150 (1981).

22. D. L. Wood and J. S. Shirk, J. Am. Cer. Soc. 64, 325 (1981).

23. B. E. Deal and A. S. Grove, J. Appl. Phys. 36, 3770 (1965).

24. E. J. Janssens and G. J. Declerck, J. Electrochem. Soc. 125, 1696 (1978).

25. B. R. Singh and P. Balk, J. Electrochem. Soc. 126, 1288 (1979).

26. Y. J. van der Meulen and J. G. Cahill, J. Electronic Materials 3, 371 (1974).

27. E. P. EerNisse and C. B. Norris, J. Appl. Phys. 45, 5196 (1974).

28. R. F. DeKeersmaecker and D. J. DiMaria, J. Appl. Phys. 51, 1085 (1980).

29. C. W. Magee, W. L. Harrington, and R. E. Honig, Rev. Sci. Instrum. 49, 477 (1978).

30. R. O. Gale, Ph.D. Dissertation, Lehigh University, Bethlehem, PA (1984).

31. C. W. Magee and W. L. Harrington, Appl. Phys. Lett 33(2), 15 (1978).

32. D. L. Griscom and E. J. Friebele, Phys. Rev. B24, 4896 (1981)

33. D. P. Leta and G. M. Morrison, Anal. Chem. 52, 514 (1980).

34. J. W. Rouse, Ph.D. Dissertation, Stanford University, Stanford, CA (1981).

35. R. O. Gale, F. J. Feigl, C. W. Magee, and D. R. Young, J. Appl. Phys. 54, 6938 (1983).

36. F. L. McCrackin, NBS Tech. Notes, No. 242, 363 (1963).

37. C. W. Magee and R. E. Honig, Surface and Interface Analysis 4, 35 (1982).

38. J. F. Gibbons, W. S. Johnson, and S. M. Mylroie, Projected Range Statistics in Semiconductor and Related Materials, 2nd ed. Academic Press, New York, 1975.

39. T. E. Seiden, in VLSI Technology S. M. Sze editor, p. 250.

40. $D=10^{-10}cm^2/sec$ at 950°C. Private communication with H. A. Schaeffer. For diffusivity at 750°C see H. A. Shaeffer and J. Steinmann, J. Am. Cer. Soc. 62, 343 (1979).

41. D. J. DiMaria, D. R. Young, W. R. Hunter and C. M. Serrano, IBM J. Res. Dev. 22, 289 (1978).

42. R. H. Doremus, Glass Science, J. Wiley and Sons, New York, 1973, Chapter 4.

43. A. S. Vengurlekar and V. P. Salvi, J. Electrochem. Soc. 132, 1172 (1985).

44. A. H. Van Ommen, J. Appl. Phys. 56, 2708 (1984).

45. A. H. Van Ommen, J. Appl. Phys. 57, 1872 (1985).

46. A. H. Van Ommen, J. Appl. Phys. 57, 5220 (1985).

47. C. Wolowodiuk, M. S. Thesis, Lehigh University, Bethlehem, PA (1985).

48. Private Communication with J. B. MacChesney, AT&T Bell Labs, Murray Hill, NJ.

49. W. A. Tiller, J. Electrochem. Soc. 128, 689 (1981).

50. R. B. Fair, J. Electrochem. Soc. 128, 1360 (1981) and references from therein.

51. J. Blanc, Semiconductor Characterization Techniques, ed. P. A. Barnes and G. A. Rozgonyi, Proceedings 78/3, p. 139, Electrochemical Society.

52. E. P. EerNisse, Appl. Phys. Lett. 30, 290 (1977).

53. E. A. Irene and J. Angilello, J. Electrochem. Soc. 129, 2594 (1982).

54. A. R. Silin, P. J. Bray and J. C. Mikkelsen Jr., J. Non-crystalline Solids 64, 186 (1984).

55. Min-Ron Lin, R. W. Dutton and W. A. Tiller, J. Electrochem Soc. 128, 1121 (1981).

56. A. S. Vengurleakar and K. V. Ramanathan, Thin Solid Film 114, 285 (1984).

Appendix I. Chlorine concentration vs. depth profiles for other compositions in Table 2-1.

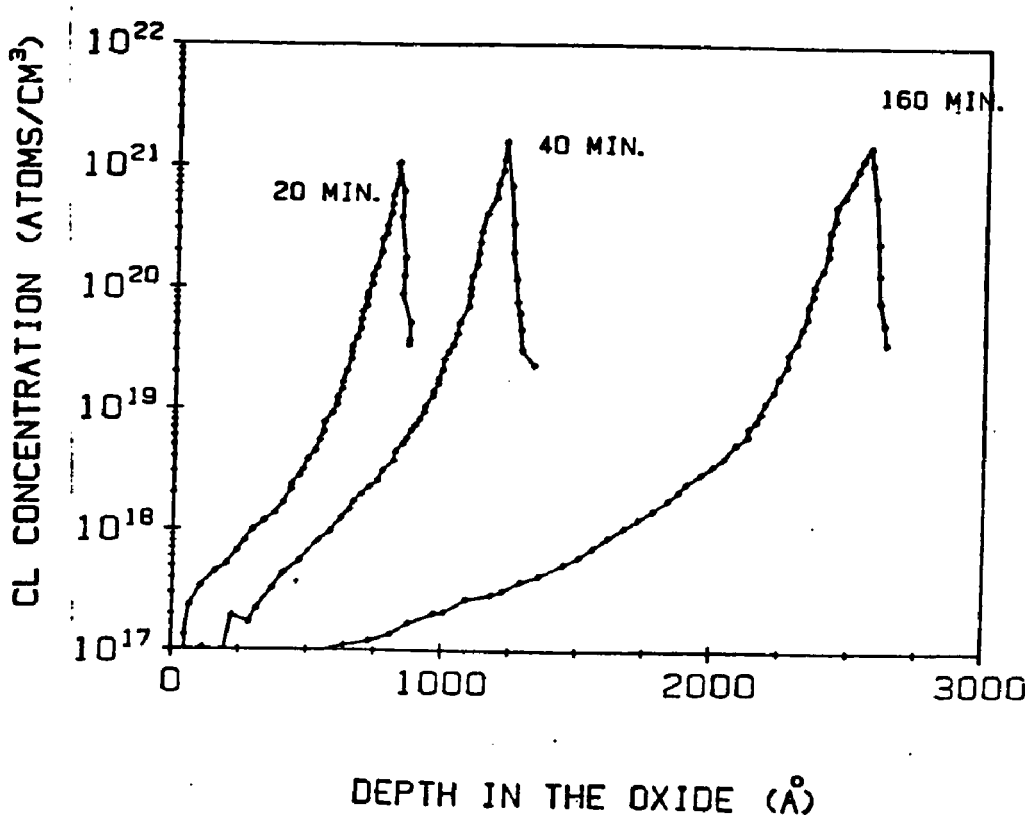

Fig. I-1 Chlorine profiles for samples with concentration "B" from Table 2-1.

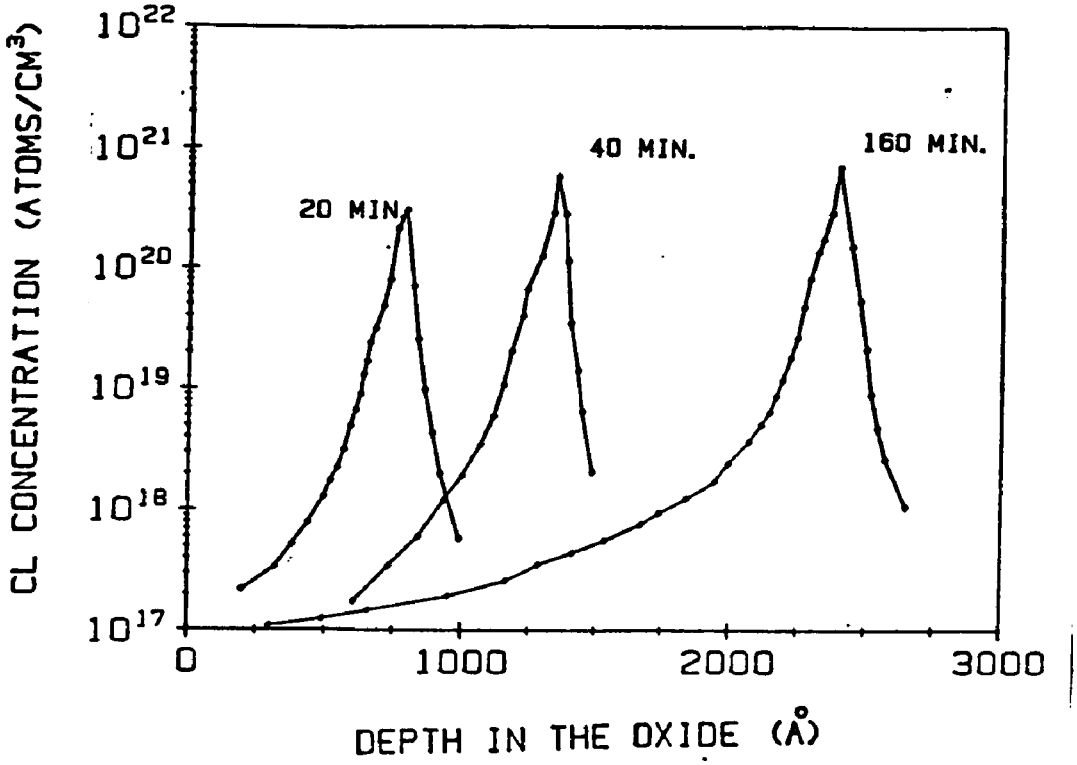

Fig. I-2 Chlorine profiles for samples with concentration "C" from Table 2-1.

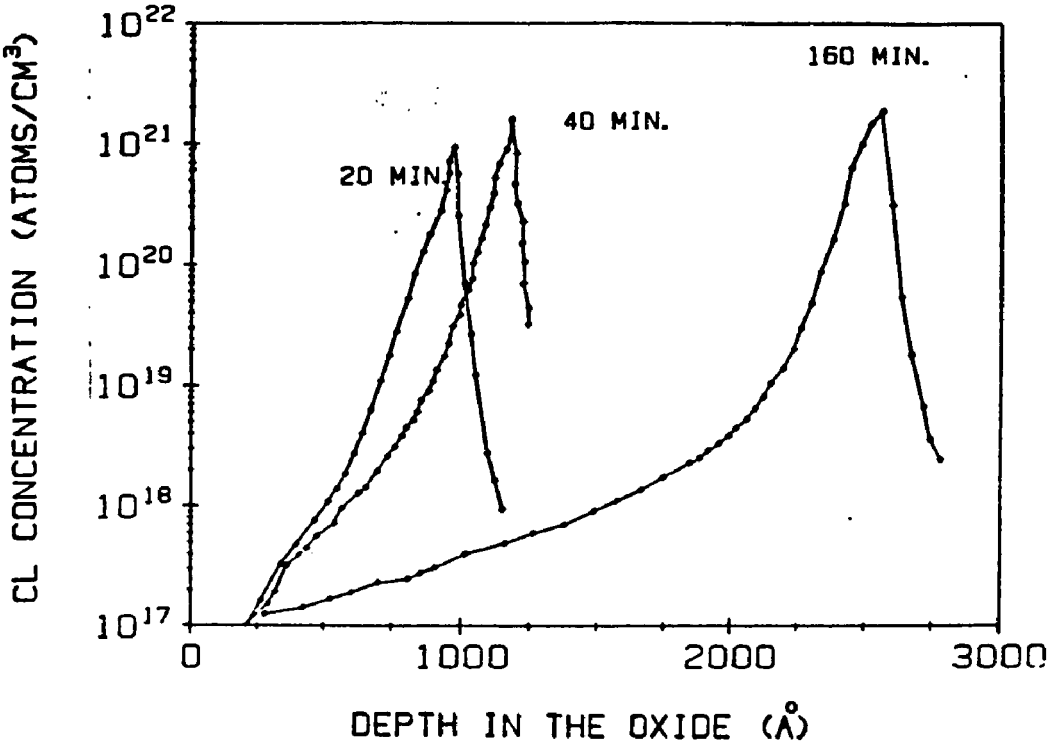

Fig. I-3 Chlorine profiles for samples with concentration "D" from Table 2-1.

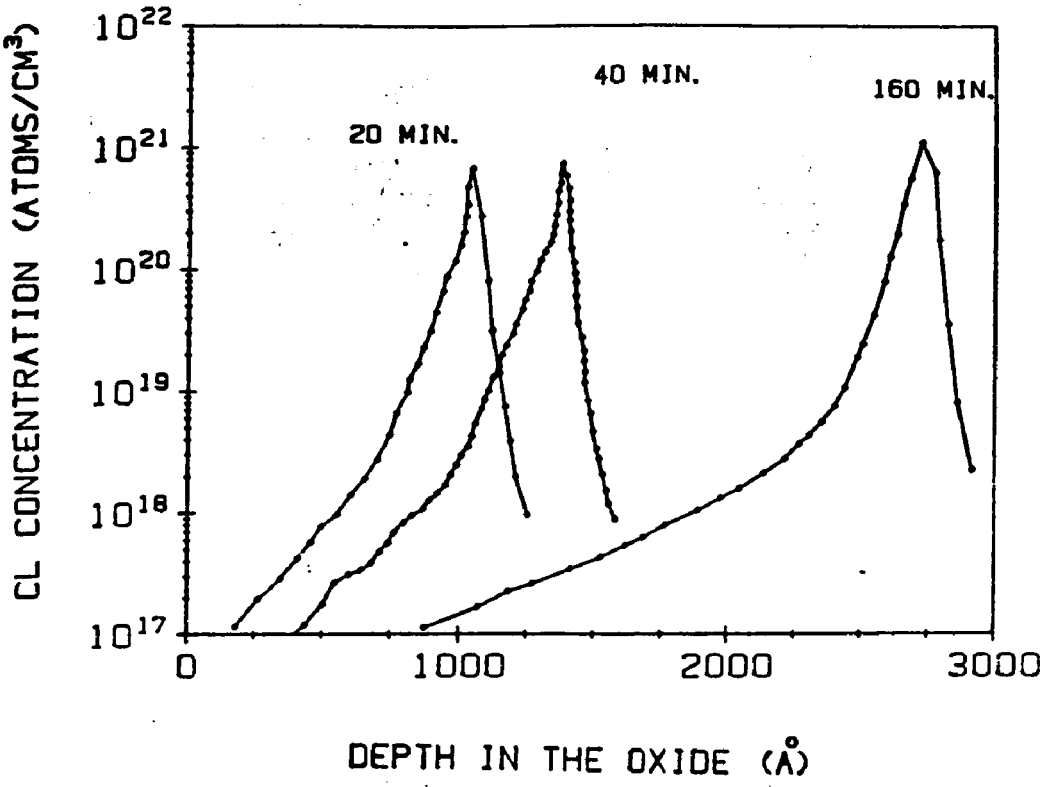

Fig. I-4 Chlorine profiles for samples with concentration "E" from Table 2-1.

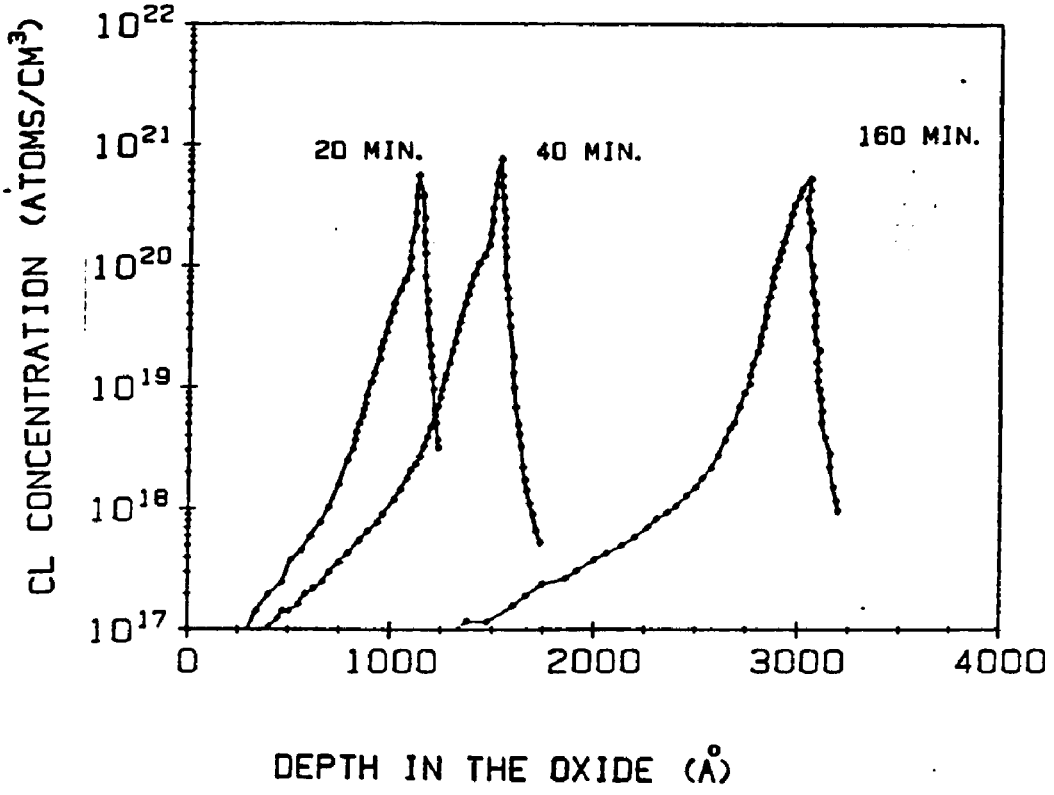

Fig. I-5 Chlorine profiles for samples with concentration "F" from Table 2-1.

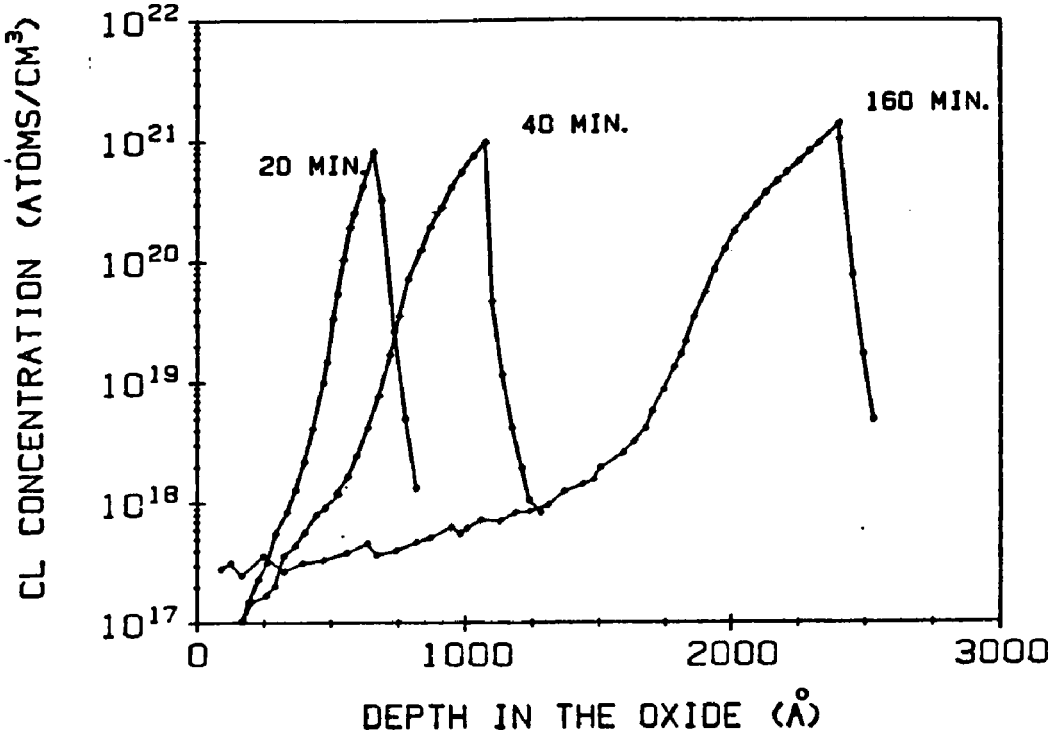

Fig. I-6 Chlorine profiles for samples with concentration "H" from Table 2-1.

Appendix II: Chlorine concentration vs. depth profiles for Cl-implanted oxide after sequential annealing in dry oxygen or O_2 + 2% H_2O.

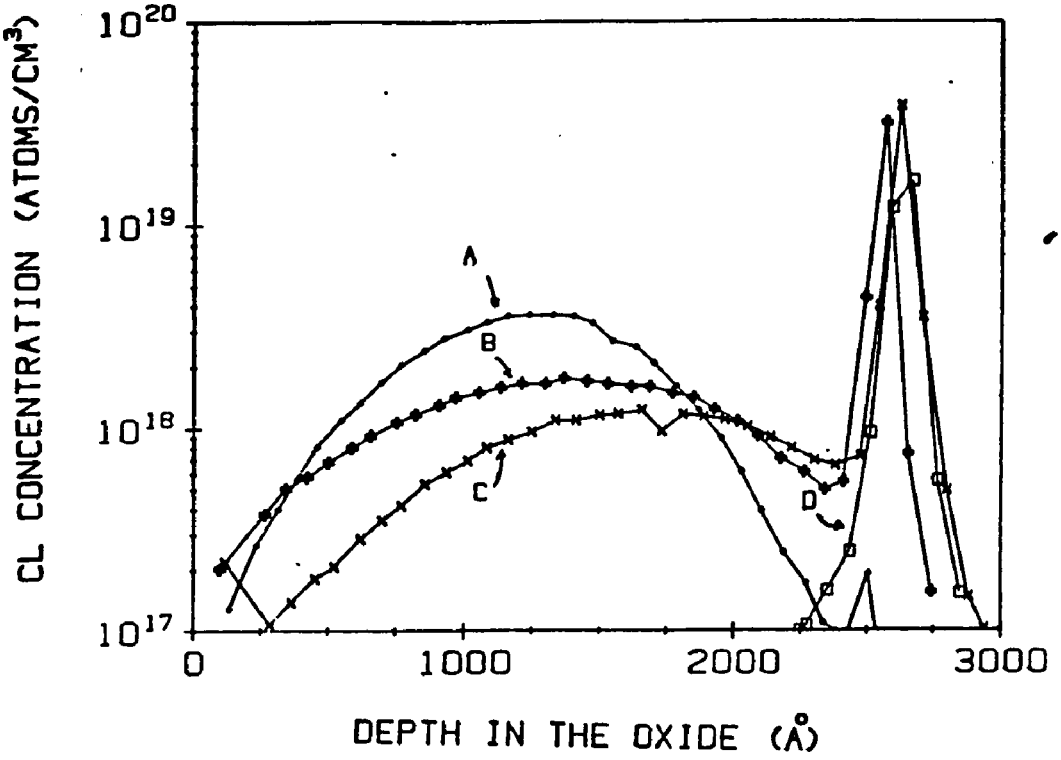

Fig. II-1 Chlorine concentration vs. depth profiles for Cl implanted oxides. All samples annealed at 600°C for 30 min. in N_2. Subsequent heat-treatment in dry oxygen at 900°C:

A, none
B, 20 min
C, 40 min
D, 60 min

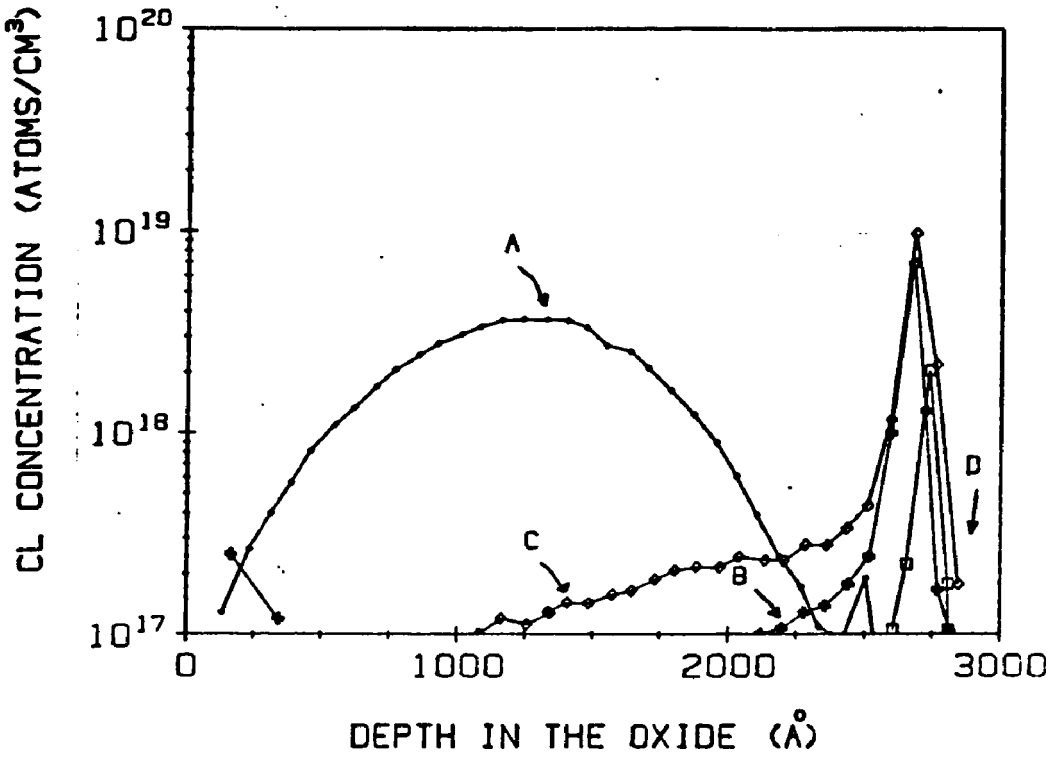

Fig. II-2 Chlorine concentration vs. depth profiles for Cl implanted oxides. All samples annealed at 600°C for 30 min in N_2. Subsequent heat-treatment in O_2 + 2% H_2O.

A, none
B, 20 min
C, 40 min
D, 60 min

Appendix III: Calibration Procedure in SIMS Analysis

The calibration was carried out using a computer program written by R. O. Gale. This program consists of the following three subroutines.

S - integrate standard
P - integrate unknown
C - convert file

The required information for input and output for these three subroutines are also summarized in this program as follows:

Integrate standard is used to find the 'fudge factor' for Cl profiles generated by SIMS and filed using 'digitize'.

This segment expects the data to be in the form of 'sputtering time (sec)', 'intensity (log(CTS/SEC))'.

User inputs include file name, background (CTS/SEC), gated area dimensions (microns), and dose (#cm^{-2}). Output consists of a single number, CL (35 and 37, assuming natural isotopic abundance) sputtered per count detected.

The integrate unknown segment is designed to find areal density of chlorine (total) from files created by 'digitize' from SIMS analyses.

User inputs include file name, background, sputtering rate, and efficiency, output is a single number, the areal density of chlorine for the profile.

Convert files is used to massage 'unknown' SIMS profiles created by 'digitize'.

Data is expected to be in the form of 'sputtering time (sec)', intensity (log CT/SEC) .

User inputs include file name, background, sputtering rate, fudge factor, output format, and output file name. Output consists of a disk file containing the converted data in the form of concentration vs. depth. See file structure.

The calculations used in this program are illustrated as follows:

List of Symbols

S	sputtering rate	(Å/sec)
α	gate size	(cm^2)
b	major constituent signal	(count/sec)
q	minor constituent signal	(count/sec)
t	cycle length	(sec)
d	dose	(atoms/cm^2)
e	background	(count/sec)

First, we determine the background e in the standard, then integrate the background subtracted signal in the standard:

$$\sum_{t_i} (q_i - e_i)t_i = Q$$

The total number of implanted atoms in the gated area N is determined by N = dose x area

$$= d\alpha$$

Then the efficiency = $(N/Q)^{-1} = \Sigma\frac{(q-e)t}{d\alpha}$

$$= \frac{\text{counts recorded}}{\text{ion sputtered from the analyzed area}}$$

The fudge factor in the standard:

$$(\text{Y-fudge})_S \equiv N/Q \text{ (atom/count)/s} \cdot \alpha(\text{cm/sec} \cdot \text{cm}^2)$$

$$= \frac{d\alpha}{\Sigma(q-e)t}/(S \cdot \alpha)$$

$$= \frac{\partial}{[\Sigma(q-e)t]S} \frac{(\text{atom/cm}^3)}{(\text{count/sec})}$$

The fudge factor in the unknown can be obtained by normalizing to the major consituent:

$$(Y - \text{fudge})_U = \left(\frac{b_s}{b_u}\right) (Y - \text{fudge})_S$$

where b_s, b_u are the major constituents in the standard and unknown, respectively.

Appendix IV: Chlorine profiles for samples prepared by oxidation at 1200°C in 2% HCl.

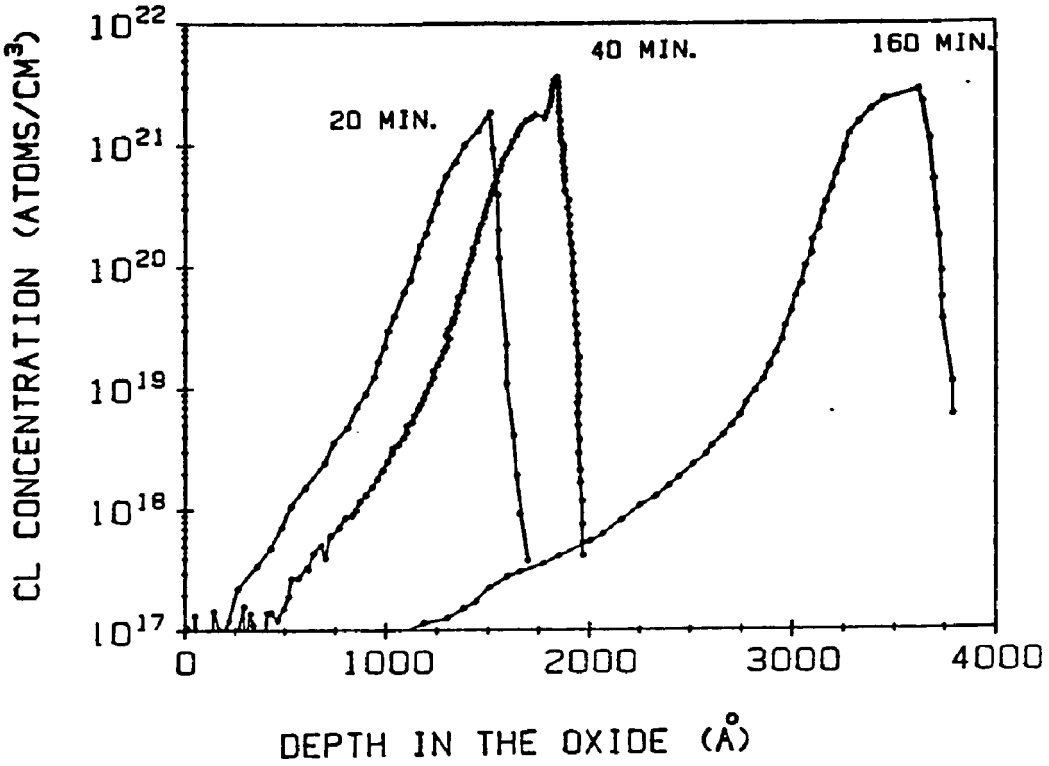

Appendix V: Heat treatment of the Cl incorporated during the thermal oxidation of Si.

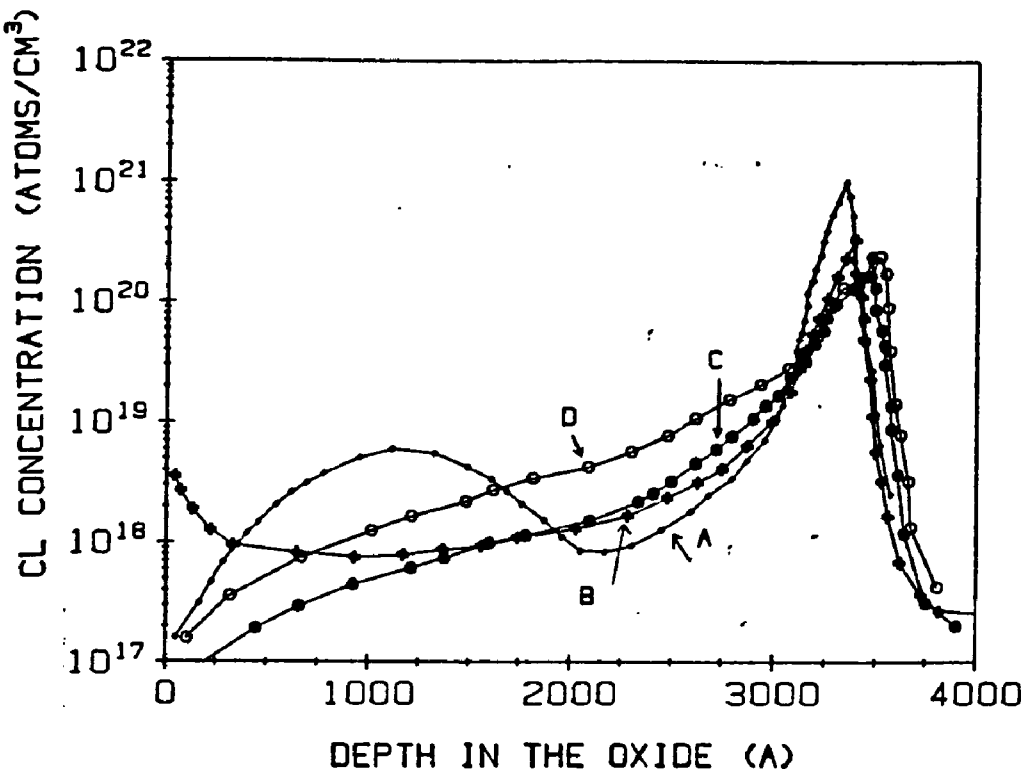

Fig. V Chlorine concentration vs. depth profiles for Cl incorporated during the thermal oxidation of Si. Subsequent heat treatment in O_2 + 2% H_2O for

A, none
B, 20 min.
C, 40 min.
D, 60 min.

VITA

The author was born on December 3, 1953, in Tainan, Taiwan. He received his B.S. degree in materials science from National Tsing Hua University in 1976. From July 1976 to May 1978 he served as a reserve officer in the Army of Taiwan.

In 1978 the author came to the United States to begin his graduate studies at Marquette University, Milwaukee, Wisconsin. He received his M.S. degree in materials science in August 1980.

The author entered the PhD program in Metallurgy and Materials Engineering of Lehigh University in the fall of 1980. He served as a physics teaching assistant from fall 1980 to fall 1981. The author has been the recipient of a National Science Foundation grant and a Sherman Fairchild Fellowship from fall 1981 to the present time.